Bistable buckled beam: Elastica modeling and analysis of static actuation

B. Camescasse, Amâncio Fernandes, J. Pouget

▶ **To cite this version:**

B. Camescasse, Amâncio Fernandes, J. Pouget. Bistable buckled beam: Elastica modeling and analysis of static actuation. International Journal of Solids and Structures, 2013, 50 (19), pp.2881-2893. 10.1016/j.ijsolstr.2013.05.005 . hal-03767869

HAL Id: hal-03767869

https://hal.sorbonne-universite.fr/hal-03767869v1

Submitted on 2 Sep 2022

HAL is a multi-disciplinary open access archive for the deposit and dissemination of scientific research documents, whether they are published or not. The documents may come from teaching and research institutions in France or abroad, or from public or private research centers.

L'archive ouverte pluridisciplinaire **HAL**, est destinée au dépôt et à la diffusion de documents scientifiques de niveau recherche, publiés ou non, émanant des établissements d'enseignement et de recherche français ou étrangers, des laboratoires publics ou privés.

Bistable buckled beam : Elastica modelling and analysis of static actuation

B. Camescasse[a,b], A. Fernandes[a,b,*], J. Pouget[a,b,**]

[a] *UPMC Univ Paris 06, UMR 7190, Institut Jean Le Rond d'Alembert, F-75005 Paris, France*
[b] *CNRS, UMR 7190, Institut Jean Le Rond d'Alembert, F-75005 Paris, France*

Abstract

We propose the modelling of a buckled elastic slender beam based on elastica approach. The model accounts for large rotations of the beam cross-section and rather large elastic displacements. Moreover, the model incorporates the extensibility of the elastic beam. The nonlinear nature of the model is used to amplify the transition from one stable position of the buckled beam to the other one. Such mechanical structure is said bistable. The bistable beam is simply supported at each of its ends and is subject to a transverse force applied at a point of the beam. The emphasis is placed especially on the bistable mechanism response caused by the applied force. The stability of the buckled beam is investigated in details and the diagram of the applied force of actuation as function of the midpoint displacement is discussed according to the applied force location. The snap-through phenomenon scenario is analyzed. The switching from one stable state to the other one occurs passing through an instability region in which the second buckling mode is involved. For rather small end shortening of the beam, the post buckling behavior is studied by reducing the solution of the complete elastica model to the first two buckling modes. The reduced model allows us to discuss the switching path in terms of energy required and stability properties of the bistable mechanism. Numerical algorithms are developed in order to solve the strongly nonlinear problem.

Keywords: Bistable system, elastica, buckled beam, optimal actuation, snap-through, nonlinear.

1. Introduction

In a previous work the snap-through mechanism of an elastic bistable beam was examined and compared to experimental validations (Cazottes et al. , 2010). Especially, the study investigates the force actuation of a bistable structure consisting of a stainless steel buckled beam. Experimental evidences exhibit the transition from one stable position of the buckled beam to the other one passing through a region of instability. It is shown that the combined buckling modes one and two can also be of value (lower snapping force and larger stable

*Corresponding author
**Principal corresponding author
Email addresses: amancio.fernandes@upmc.fr (A. Fernandes), pouget@lmm.jussieu (J. Pouget)

domain) and should be considered for mechanical design. The purpose of the present study is to investigate the switching mechanism of a bistable buckled beam on the basis of elastica model. More precisely, we examine in details the stability of the buckled beam undergoing a local force actuation in the post-buckling regime. One of the main results that we want to achieve is to understand the mechanism of snapping from one stable position to the other one according to the actuation force and the influence of the actuation location on the performances of the system.

Bistable mechanisms make them very attractive candidates to design systems that require two working states. The switching from one state to the other one needs low energy. Bistable systems are often used as switches (Saif , 2000; Brenner et al. , 2003). They are also used in microrobotic applications such as microgrippers or binary robotic devices (Fang and Wickert , 1994; Schomburg and Groll , 1998; Reni and Gerhard , 1997). A promising application is quasitactile display with high density matrix of tiny pins with excellent spatial resolutions (Jensen et al. , 1999; Benali-Khoudja et al. , 2007; Hafez , 2007). Haptic applications can be considered as well. One of the advantages of bistable systems is that they need substantial energy during the switching process. Indeed, they take advantage of the instability phenomena, a rather small of amount of actuating work can produce displacements or rotations of the slenderness structure of relatively high amplitudes. Once the actuation is released, the system stays in its stable configuration indefinitely. This property is exploited to the design of shape control devices (Baker and Howell , 2002).

Other categories of mechanisms use their elastic deformation as a function. Bistable systems belong to this kind of mechanisms. Among a various nonlinear problems analyzed in the literature, bistable systems consisting in buckled elastic beams have received a great deal of attention due to their quite rich nonlinear behavior and their attractive applications. A rather rough, nevertheless really instructive, example of bistable system consists of rigid barres, springs and masses. This class of bistable system is referred as to pseudo rigid category (McInnes and Waters , 2008). In (Pucheta and Cardona , 2010), the authors present an interesting study devoted to the design of bistable compliant mechanisms based on various pseudo-rigid models with some instructive applications. Numerous studies on bistable systems are available in the current literature and modelling of systems depends strongly on the hypotheses concerning kinematic description and the degrees of sophistication of the approaches. Important foundation of the large-displacement finite-strain approach of shear-deformable beams has been laid down by Reissner (Reissner , 1972). Reissner has extended his beam approach for the plane case of shear-deformable and extensible nonlinear beams to 3D-curved beams (Reissner , 1973). A restricted situation of the Reissner's approach to unshearable nonlinear beam originally straight has been extensively presented by Irschik and Gerstmayr (Irschik and Gerstmayr , 2009). On the basis of (Irschik and Gerstmayr , 2009), Hummer and Irschik (Hummer and Irschik , 2011) examined the equilibrium configurations and stability of an extensible elastic with an unknown

length.

Numerous contributions to problem dealing with bistable structures are based on elastic theory of flexible beams. In (Patricio et al. , 1998), the authors analyzed the modes of stability of an elastic homogeneous arch loaded at its center on the basis of elastica theory. The stability of dynamics perturbations around static state leads to stability diagram according to the end-shortening of the beam and frequency. Nevertheless, the elastic model is supposed to be inextensible. Experimental study of elastic arch loaded at its center was performed by Pippard (Pippard , 1990). In (Magnusson et al. , 2001), the authors examined the behavior of a pinned-pinned axially beam in the extensible framework. In the approach, the authors study very clearly the buckling and post-buckling behavior of the beam, and they extended their beam theory of Euler-Bernoulli for elastic beams to small displacements in order to account for large-displacement and finite-strain.

Among various nonlinear studies analyzed in literature, buckled elastic beams have received particular attention due to their complex and rich dynamics responses to different kind of stimuli. In this context, weakly nonlinear approach is often considered, in (Nayfeh and Enam , 2008), the authors accounts for the geometric nonlinearity arising from the mid plane stretching of the buckled beam. They derived the governing equation of the transverse vibrations exhibiting a cubic nonlinearity. Along with this approach, the dynamic stability of the post-buckling solutions is investigated. A simply supported shallow arch was examined by Pinto and Gonçalves (Pinto and Gonçalves , 2002) for instability phenomena when the structure undergoes dynamic and static loads, in particular, snap-through buckling. The model used considers a weakly nonlinear geometric behavior of an arch due to the beam extensibility. Among works found in recent literature, most of them are mainly devoted to the snap-through effect of a buckled elastic micro-beams and their actuation. Interesting studies of the phenomenon at the micro-scale are presented in (Buchaillot et al. , 2008; Krylov and Dick , 2010; Krylov et al. , 2011) with applications to MEMS, micro robotics, micro-opto-electro-mechanical systems.

A weakly nonlinear behavior of the snap-through of compressed bistable buckled beam was investigated by Vangbo (Vangbo , 1998) by considering the Lagrangian approach under constraint. The energy associated with both bending and compression of the beam is expanded using the buckling modes of a clamped-clamped beam. The author characterized the bistablility response due to a control loading. Qiu et al. (Qiu et al. , 2004) extended the method to a bistable system made of two centrally-clamped parallel beams. Application to a tunable micromechanical bistable system was examined on the basis of Vangbo's work (Taher and Saif , 2000).

The proposed approach relies on the extensible elastica model where the beam kinematics is described in terms of the cross-sectional rotations. The equations of the model as well as the jump conditions at the point of the force application are derived from the virtual work principle. It is also shown that the model can be deduced from a Lagrangian formulation. The conditions

at the ends of the beam are well formulated and the model parameters are well identified. Especially, the axial compressive force and the actuating transverse force are considered as unknown parameters of the problem which are solved by using the end shortening condition and the vertical coordinate location of the actuating force. The set of equations are then solved by means of shooting numerical method associated with a predictor-corrector algorithm to capture the unknown model parameters (or the shooting unknowns). From the numerical investigation new results are obtained and discussed, among them, the response diagram of the actuating force as function of the driving point or the beam mid-point. Moreover, a detailed discussion of the configurational stability of the bistable system is presented in terms of buckling modes. The analysis of the post-buckling regime of the bistable is investigated by using a reduced order model limited to first two buckling modes.

2. Description of the system

We consider an elastic beam of length L_0 at the rest. The beam is simply supported at each of its ends. The left end is fixed while the right one can move along the beam axis. The cross-section of the beam is supposed to be rectangular with a width b and thickness h. The beam is subject to an end-shortening ΔL that reduces the distance between the pin-joints. The distance becomes $\hat{L} = L_0 - \Delta L$. The end-shortening ΔL will play a crucial role in the buckling process of the elastic beam. The elastic beam at the rest and in the buckled configuration along with the parameters are depicted in Figure 1. The elastic beam is initially straight when it is stress free. The beam undergoes a deformation due to the end-shortening and deflection can take place in the beam plane, i.e. the (xAy) plane.

The buckled beam is loaded by a localized force F in the y-direction. The abscissa of the point C at which the force is applied is maintained fixed while the beam is snapping-through. The ratio $\hat{\delta} = \frac{x_C - x_A}{x_B - x_A} = \frac{x_C}{\hat{L}}$ is a key parameter of the problem.

The elastic beam is supposed to be materially homogeneous with Young modulus E and mass density ρ. We denote by I the moment of inertia of the cross-section along z-axis.

3. Modelling

3.1. Kinematics and deformation descriptions

Geometric considerations - Before entering detailed considerations of the problem under study, some basic prerequisites and assumptions must be introduced and commented. Accordingly, we attach a fixed Cartesian reference frame $(\vec{e}_1, \vec{e}_2, \vec{e}_3)$ to the structure in its initial configuration referred as to $\mathcal{R}_0$. The x-axis coincides with the axis of the beam which is supposed to be straight in the reference or underformed configuration. In addition, y represents the thickness coordinate of the beam and the z-axis is perpendicular to plane deformation, see Figure 2. The deformation is assumed to take place in $(\vec{e}_1, \vec{e}_2)$-plane. Any material point G_0' of the beam in the reference configuration $\mathcal{R}_0$, is given by its position

$$\overrightarrow{OG'_0} = \overrightarrow{OG_0} + y_0\vec{e}_2, \tag{1}$$

The transverse coordinate z_0 has been omitted since it plays no role in the beam deformation. We note by s the curvilinear abscissa along the beam axis in the reference configuration. The position of the material point G_0 belonging to the beam axis is given by

$$\overrightarrow{OG_0} = \vec{q_0}(s) = s\vec{e}_1, \quad \text{with} \quad s \in [0, L_0] \tag{2}$$

where $\vec{q_0}$ is the position vector in the reference configuration. The plane deformation of the beam is ascertained if the loading and the joints at the beam ends are symmetric with respect to the $(\vec{e}_1, \vec{e}_2)$-plane.

The material point G'_0 is transformed into G' after beam deformation in the current configuration $\mathcal{R}$ (or deformed state, see Figure 2). The position of the material point G' is now given by the position vector

$$\overrightarrow{OG'} = \overrightarrow{OG} + \overrightarrow{GG'}, \quad \text{with} \quad \overrightarrow{OG} = \vec{q} = x\vec{e}_1 + y\vec{e}_2. \tag{3}$$

The actual position of the material point G' is then function of the coordinates in the reference configuration (Lagrangian description), especially, it depends on s and y_0.
Now, we formulate the Euler-Bernoulli assumptions, that is, the cross-sections originally perpendicular to the beam axis in the reference configuration remain perpendicular to the axis in the deformed state, plane and undistorted, as well. The material point G_0 belonging to the beam axis in the reference configuration is transformed into the material point G of the beam axis in the deformed state. We denote by $\vec{\tau}$ the unit vector tangential to the current axis of the deformed beam at the point $G\,(\bar{s})$. The vector $\vec{\tau}$ is usually defined by

$$\vec{\tau} = \frac{d\overrightarrow{OG}}{d\bar{s}}. \tag{4}$$

Nevertheless the position vector $\vec{q}$ of the material point G is a function of the reference coordinate, especially function of the curvilinear abscissa s. We denote by $\Lambda = \frac{d\bar{s}}{ds}$ the ratio of the length of differential line element of the beam axis in the deformed state to that of the undeformed configuration. Eqn. (4) becomes

$$\frac{d\overrightarrow{OG}}{ds} = \Lambda\vec{\tau}. \tag{5}$$

Denoting by $\vec{n}$ the unit vector perpendicular to the tangent vector $\vec{\tau}$, the set of orthogonal vectors $\{\vec{\tau}, \vec{n}\}$ forms the local frame attached to the deformed beam axis at the curvilinear abscissa $\bar{s}$ (see Figure 2). These vectors can be written with respect to the fixed referential $\{\vec{e}_1, \vec{e}_2\}$

$$\begin{cases} \vec{\tau}(s) = \cos\theta(s)\ \vec{e}_1 + \sin\theta(s)\ \vec{e}_2 \\ \vec{n}(s) = -\sin\theta(s)\ \vec{e}_1 + \cos\theta(s)\ \vec{e}_2 \end{cases} \tag{6}$$

where the angle of rotation θ is given by

$$\theta = (\vec{e}_1, \vec{\tau}). \tag{7}$$

Moreover, in the current configuration, the cross-sections are rotated by the angle θ about the z-axis with respect to the reference configuration.

Now, the position vector of any material point G' of the cross-section in the deformed state takes on the form (see Eqn. (3))

$$\overrightarrow{OG'} = \vec{q} + y_0\vec{n}. \tag{8}$$

The coordinate of the position vector of the point G, $\vec{q} = (x, y)$ in the current configuration are function of the curvilinear abscissa s measured along the beam axis. Therefore, the current configuration of the beam is a smooth curve defined by

$$\mathcal{C}(s) = \{\vec{q}(s) = x(s)\ \vec{e}_1 + y(s)\ \vec{e}_2,\ s \in [0, L_0]\}, \tag{9}$$

One of the kinematic key parameters of the deformed beam is its curvature κ. The curvature of a line element $d\bar{s}$ of the beam axis is usually defined by (Reissner , 1972; Simo , 1985),

$$\kappa = \left|\left|\frac{d\vec{\tau}}{d\bar{s}}\right|\right| = \frac{1}{\Lambda}\left|\left|\frac{d\vec{\tau}}{ds}\right|\right|. \tag{10}$$

On using Eqn. (6) we compute

$$\frac{d\vec{\tau}}{ds} = \theta_{,s}\vec{n}. \tag{11}$$

Accordingly, we obtain the following equation for the beam curvature

$$\kappa = \frac{1}{\Lambda}\frac{d\theta}{ds}. \tag{12}$$

The factor Λ is sometimes missing in elastic theory for extensible elastic beam. On using the curvilinear abscissa $\bar{s}$ measured along the deformed beam axis, the curvature takes on the following form

$$\kappa = \theta_{,\bar{s}}. \tag{13}$$

Remark. For inextensible elastic theory, obviously $\Lambda = 1$ and we cannot distinguish the curvilinear abscissa s and $\bar{s}$ measured along the undeformed and deformed configurations, respectively.

Gradient of deformation - According to the above hypotheses on the beam deformation, the gradient of deformation can be written as (Eringen , 1967)

$$\mathbf{F} = \mathbf{Grad}\ \overrightarrow{OG'} = \frac{\partial \overrightarrow{OG'}}{\partial s} \otimes \vec{e}_1 + \frac{\partial \overrightarrow{OG'}}{\partial y_0} \otimes \vec{e}_2, \tag{14}$$

where **Grad** is the gradient of the transformation computed with respect to the reference configuration. Now, by using Eqns. (3, 6, 8, 11, 12) , we arrive at

$$\mathbf{F} = \Lambda \left(1 - y_0 \kappa\right) \vec{\tau} \otimes \vec{e}_1 + \vec{n} \otimes \vec{e}_2. \tag{15}$$

Next, we compute the component of the gradient of deformation in the basis of the reference configuration by using Eqn. (6), which can be presented in the matrix form

$$\mathbf{F} = \begin{bmatrix} \Lambda \left(1 - y_0 \kappa\right) \cos\theta & -\sin\theta \\ \Lambda \left(1 - y_0 \kappa\right) \sin\theta & \cos\theta \end{bmatrix} \tag{16}$$

From Eqns. (3, 5) and (6), we compute the gradient of deformation of the beam axis relative to the beam curvilinear coordinate

$$\begin{cases} x_{,s}(s) &= \Lambda(s) \cos\theta(s) \\ y_{,s}(s) &= \Lambda(s) \sin\theta(s) \end{cases} \tag{17}$$

The gradient of deformation possesses a unique polar decomposition of the form (Eringen , 1967) $\mathbf{F} = \mathbf{RU}$, where $\mathbf{R}$ is an orthogonal tensor of rotation such that $\mathbf{RR}^T = \mathbf{R}^T\mathbf{R} = \mathbf{1}$, and $\mathbf{U}$ is the symmetric tensor of the right stretch. On using the matrix form of the gradient of deformation given by Eqn. (16), we are able to identify the polar decomposition with

$$\mathbf{R} = \begin{bmatrix} \cos\theta & -\sin\theta \\ \sin\theta & \cos\theta \end{bmatrix} \tag{18}$$

We note that $\mathbf{R}\left(\theta\right)^T = \mathbf{R}\left(-\theta\right)$. In addition, the stretch tensor takes on the form

$$\mathbf{U} = \begin{bmatrix} \Lambda \left(1 - y_0 \kappa\right) & 0 \\ 0 & 1 \end{bmatrix} \tag{19}$$

Now it is clear that the tensor $\mathbf{U}$ is definite positive and it possesses two distinct eigenvalues

$$U_1 = \Lambda \left(1 - y_0 \kappa\right), \quad U_2 = 1. \tag{20}$$

The associated eigenvector are obviously $\vec{e}_1$ and $\vec{e}_2$, which are the principal directions of stretch. From the physical point of view, U_1 is the principal stretch of a material line element ds parallel to the beam axis in the reference configuration and Λ is merely the axis stretch. Therefore, the beam deformation is the combination of a stretch of the beam axis follows by a rotation of angle θ described by the tensor of rotation $\mathbf{R}\left(\theta\right)$.

Moreover, the tensor of rotation can be written as

$$\mathbf{R} = \vec{\tau} \otimes \vec{e}_1 + \vec{n} \otimes \vec{e}_2. \tag{21}$$

Now using the polar decomposition with the forms of the stretch tensor and the tensor of rotation, the gradient of deformation can be written as

$$\mathbf{F} = U_1 \left(\vec{\tau} \otimes \vec{e}_1 \right) + U_2 \left(\vec{n} \otimes \vec{e}_2 \right). \tag{22}$$

This shows that the principal stretches give the ratio of length of material line elements in the deformed configuration relative to that of the reference configuration.

Distributor of transformation - The two strain measures of the beam model are given by the extensional strain $\varepsilon = \Lambda - 1$ and the beam curvature $\kappa = \theta_{,\bar{s}}$. Using these definitions for the beam deformation, we introduce the *distributor of the beam transformation* that the components are the actual position of the current point G, $\overrightarrow{OG} = x(s)\ \vec{e}_1 + y(s)\ \vec{e}_2 = \vec{q}(s)$ and the rotation $\vec{p}(s) = \theta(s)\ \vec{e}_3$ of each cross-section at the current point of the curvilinear abscissa s. Therefore, it is necessary to define the following *distributor of transformation gradient*

$$\left\{ \frac{d\mathcal{U}}{ds} \right\}_{G(s)} = \frac{d}{ds} \left\{ \begin{array}{c} \vec{p}(s) \\ \vec{q}(s) \end{array} \right\}_{G(s)} \tag{23}$$

The different deformation measures which have been introduced in this Section will be very convenient to deduce the beam equations.

3.2. Elastica beam variational formulation

With the aim at deducing the beam equations, we adopt the principle of virtual works. The principle for the present model of beam and configuration is stated as follows

$$\delta\mathcal{W}_i + \delta\mathcal{W}_e + \delta\mathcal{W}_\lambda = 0. \tag{24}$$

The different contributions to the principle are denoted by $\mathcal{W}_i$ for the work of the internal forces, $\mathcal{W}_e$ for the work of the applied actions and $\mathcal{W}_\lambda$ for the work of the eventually constraints on the kinematic variables. The expression of the virtual works in Eqn. (24) are given in details in the next subsections.

3.2.1. Internal virtual work

The virtual work of internal forces reads as

$$\delta\mathcal{W}_i = -\int_0^{L_0} \left\{ \mathcal{T}(s) \right\}_{G(s)} \cdot \frac{d}{ds} \left\{ \delta\mathcal{U}(s) \right\}_{G(s)} ds. \tag{25}$$

In Eqn. (25), $\left\{ \mathcal{T}(s) \right\}_{G(s)}$ is the distributor of the internal forces defined by

$$\{\mathcal{T}(s)\}_{G(s)} = \left\{ \begin{array}{c} \vec{R}(s) \\ \vec{M}(s) \end{array} \right\}_{G(s)} \tag{26}$$

where $\vec{R}(s)$ is the force resultant and $\vec{M}(s)$ is the moment computed at the point $G(s)$ of the beam. In Eqn. (25), $\{\delta\mathcal{U}(s)\}_{G(s)}$ is the virtual beam transformation as defined in the kinematic considerations.
On using Eqn. (23),

$$\left\{ \frac{d\delta\mathcal{U}}{ds} \right\}_{G(s)} = \left\{ \begin{array}{l} \delta\vec{p}'(s) \\ \delta\vec{q}'(s) + \frac{d\overrightarrow{OG}}{ds} \times \delta\vec{p}(s) \end{array} \right\}_{G(s)} \tag{27}$$

where it has been set $(\bullet)' = \frac{d\bullet}{ds}$ the spacial derivative. Now, the virtual work of internal actions can be put in the following form

$$\delta\mathcal{W}_i = -\int_0^{L_0} \left\{ \vec{R}(s) \cdot \delta\vec{q}'(s) + \vec{M}(s) \cdot \delta\vec{p}'(s) - \left(\vec{q}'(s) \times \vec{R}(s) \right) \delta\vec{p}(s) \right\} ds \tag{28}$$

3.2.2. Virtual work of the applied actions

The only force acting on the elastica beam which produces nonzero work is the actuation force $\vec{F}$ applied at the point C located at the unknown curvilinear abscissa $\bar{s}_c$ in the deformed configuration. For a virtual displacement of the point C, $\delta\vec{q}(\bar{s}_c)$, the corresponding virtual work reads as

$$\delta\mathcal{W}_e = \vec{F} \cdot \delta\vec{q}(\bar{s}_c) \tag{29}$$

where in our particular situation, we have

$$\vec{F} = -F\vec{e}_2, \qquad \delta\vec{q}(\bar{s}_c) = \delta y_c \vec{e}_2. \tag{30}$$

Remarks.

(i) Obviously, we have the actions of the simple support at the points A and B of the beam, nevertheless, these points are fixed. The modelling can be easily extended to a general boundary conditions at the ends of the beam, for instance applied forces or moments or clamped conditions at the beam ends or any other conditions.

(ii) The beam actuation can be extended to a lineic density of force or applied moment located at a fixed point of the beam; which can be easily incorporated in the formulation.

3.2.3. Virtual works of constraints

Because of the simply supported conditions at each end of the beam, geometric conditions must be fulfilled. More precisely, the point A is fixed and the point B is subject to an end-shortening of the fixed amount. The conditions are given by

$$\begin{aligned} x(0) &= 0, \quad x(L_0) = x_B, \\ y(0) &= 0, \quad y(L_0) = 0, \end{aligned} \tag{31}$$

These conditions can be conveniently replaced by integral conditions

$$\int_0^{L_0} x'(s)ds = x_B, \qquad \int_0^{L_0} y'(s)ds = 0. \tag{32}$$

The variation of the above condition leads to

$$\int_0^{L_0} \delta\vec{q}'(s)ds = \vec{0}. \tag{33}$$

Now, the problem is to find the solution to the minimization of the virtual work under the integral conditions Eqn. (32). In order to use the virtual work principle subject to the constraint Eqn. (33) on the arbitrary virtual displacement $\delta\vec{q}(s)$, we consider a Lagrange multiplier vector associated with the condition Eqn. (33). Accordingly, we introduce the virtual work due to the Lagrange multiplier

$$\delta\mathcal{W}_\lambda = \int_0^{L_0} \vec{\lambda} \cdot \delta\vec{q}'(s)ds. \tag{34}$$

The vector $\vec{\lambda} = (\lambda_x, \lambda_y)$ of which the components are the Lagrange multipliers enforcing the integral constraint Eqn. (33) associated with the boundary conditions at the ends of the beam.

3.2.4. Virtual work formulation

Variational formulation established by Eqn. (24) consists of looking the state fields in space $\mathcal{V} = \{x(s), y(s), \theta(s)\}$ and those admissible Lagrange multipliers (λ_x, λ_y) satisfying the variational Eqn. (24). On using Eqs. (28,29,34) the variational equation can be written as

$$\begin{aligned} &-\int_0^{L_0} \left\{ \vec{R}(s) \cdot \delta\vec{q}'(s) + \vec{M}(s) \cdot \delta\vec{p}'(s) - \left(\vec{q}'(s) \times \vec{R}(s)\right) \delta\vec{p}(s) \right\} ds \\ &+\int_0^{L_0} \vec{\lambda} \cdot \delta\vec{q}'(s)ds + \vec{F} \cdot \delta\vec{q}(s_c) = 0. \end{aligned} \tag{35}$$

The actuating force $\vec{F}$ applied at the curvilinear abscissa s_c of the beam produces a discontinuity in the internal force resultant $\vec{R}$ at this point. Consequently, we must split the variational Eqn. (35) into two segments of integration $[0, L_0] = [0, s_c[\cup]s_c, L_0]$. The integrals in Eqn. (35) are also separated into two integrals over the segment at the left of s_c and the segment at the right of this point. Now, by integrating by part, we arrive at the following variational equation

$$
\begin{aligned}
&\int_0^{s_c} \left\{ \frac{d\vec{R}^-}{ds} \cdot \delta\vec{q}^- + \left(\frac{d\vec{M}^-}{ds} + \vec{q}^{-\prime} \times \vec{R}^- \right) \cdot \delta\vec{p}^- \right\} ds \\
&+ \int_{s_c}^{L_0} \left\{ \frac{d\vec{R}^+}{ds} \cdot \delta\vec{q}^+ + \left(\frac{d\vec{M}^+}{ds} + \vec{q}^{+\prime} \times \vec{R}^+ \right) \cdot \delta\vec{p}^+ \right\} ds \\
&+ \left([\![\vec{R}\,(s_c)]\!] + \vec{F} \right) \cdot \delta\vec{q}(s_c) - [\![\vec{M}\,(s_c)]\!] \cdot \delta\vec{p}(s_c) = 0.
\end{aligned}
\tag{36}
$$

where we note the jump of any quantity by $[\![A]\!] = A^+ - A^-$. The above form the variational equation is now in a convenient form to deduce the beam equations.

3.3. Elastica beam equations

Before writing down the equations of the beam, for sake of consistency and in order to introduce key parameters as function of the beam characteristics, we define the following dimensionless parameters and variables

- *lengths* $\left(S, X, Y, \vec{Q}, \Delta\mathsf{L}\right) = (s, x, y, \vec{q}, \Delta L)\,/L_0.$ (37a)
- *Forces and moments* $\left(\vec{\mathsf{F}}, \vec{\mathsf{R}}, \vec{\mathsf{M}}\right) = \left(\vec{F}/F_0, \vec{R}/F_0, \vec{M}/M_0\right).$ (37b)
- *Energy* $\mathcal{E}_{tot} = E_{tot}/E_0.$ (37c)

with $F_0 = EAk$, $M_0 = EI/L_0$ and $E_0 = F_0 L_0$. In addition, we have placed a key parameter in evidence

$$
k = \frac{I}{AL_0^2} \tag{38}
$$

which characterize the ratio of the bending energy over the compression energy. The parameter $k \propto (h/L_0)^2$ with L_0/h is the slenderness ratio of the beam which plays a crucial role in the bistable mechanism. The total energy E_{tot} is defined as the sum of the flexural and compressive energies.

Therefore, the equation of the beam deduced from the variational formulation Eqn. (36) is given by

$$
\frac{d\vec{\mathsf{M}}}{dS} + \frac{d\vec{Q}}{dS} \times \vec{\mathsf{R}} = \vec{0}, \tag{39}
$$

The above equation holds for both segments of the beam. In addition, we deduce the equations of the jump at the point of actuating force for the resultant and the moment, that is

$$
\begin{aligned}
&[\![\vec{\mathsf{R}}(s_c)]\!] + \vec{\mathsf{F}} = \vec{0}, \\
&[\![\vec{\mathsf{M}}(s_c)]\!] = \vec{0},
\end{aligned}
\tag{40}
$$

The first equation of Eqn. (40) denotes that the jump of the resultant of the internal action is the actuating force while the second equation means that the bending moment is continuous across the point C.
The geometrical compatibility Eqn. (17) using the dimensionless variables can be rewritten in the vectorial form

$$\frac{d\vec{Q}}{dS} = (1+\varepsilon(S))\,\vec{\tau}. \tag{41}$$

Constitutive equations of the beam. The analysis of the bistable beam must be completed by giving the relationships between the strain measures and the resultants in force and moment. The elastic behavior of the beam is supposed to be linear. The constitutive equations are stated as

$$\vec{R}\cdot\vec{\tau} = N = EA\varepsilon(s),$$
$$\vec{M} = EI\theta_{,s}\vec{e}_3.$$

On using the dimensionless quantities, we arrive at

$$\varepsilon(S) = k\mathsf{N}, \tag{42a}$$
$$\vec{\mathsf{M}} = \frac{d\theta}{dS}\vec{e}_3. \tag{42b}$$

It is worthwhile noting that the parameter k holds for the compressibility of the beam and N is the resultant along the beam axis and perpendicular to the beam cross-section.

Remarks : The equilibrium equation (39) can be deduced from the following Lagrangian

$$\mathcal{L} = \int_0^{L_0} \left[\frac{1}{2}\vec{\mathsf{M}}\cdot\frac{d\vec{p}}{dS} + \frac{1}{2}\mathsf{N}\varepsilon - (1+\varepsilon)\,\mathsf{N}\right] dS, \tag{43}$$

where the first term in the integral Eqn. (43) is reduced to $\frac{1}{2}\vec{\mathsf{M}}\cdot\frac{d\vec{p}}{dS} = \frac{1}{2}\left(\frac{d\theta}{dS}\right)^2$ is the bending energy, $\frac{1}{2}\mathsf{N}\varepsilon$ with $\varepsilon = k\mathsf{N}$ is the compression energy. The last term in Eqn. (43) is deduced from the boundary conditions at both ends of the beam of the displacements $X(S)$ and $Y(S)$ and it involves Lagrangian multipliers. More precisely, from Eqn. (41) and Eqn. (42) we write

$$(1+\varepsilon)\,\mathsf{N} = (1+\varepsilon)\,\vec{\mathsf{R}}\cdot\vec{\tau} = \vec{\mathsf{R}}\cdot\frac{d\vec{Q}}{dS}.$$

Now, it clear, if we consider the boundary conditions on both ends of the beam in their integral form given by Eqn. (32), that the vector $\vec{R}$ can be viewed as the Lagrangian multiplier. The latter can be identified to the vector $\vec{\lambda}$ which has the meaning of a force maintaining fixed the end-shortening on the right end of beam and imposing the vertical displacements at both ends of beam to be zero.

The beam equation (39) is deduced by rendering the Lagrangian stationary, i.e., $\delta\mathcal{L} = 0$. The Lagrangian form is deduced directly from the variational equation (36) after direct algebraic manipulations. Due to the actuating force applied to the point C of the beam, the Lagrangian Eqn. (43) must be split into two integrals one over the segment $S \in [0, S_C[$ and the other one over the segment $S \in]S_C, 1]$.

3.3.1. Beam equilibrium

The global equilibrium of the beam subject to buckling load and actuating force allows to compute the unknown resultants applied at each end of the beam. The resultants are found out as follow

$$\mathsf{N}_A = \mathsf{P}, \tag{44a}$$

$$\mathsf{V}_A = (1 - \hat{\delta})\ \mathsf{F}, \tag{44b}$$

$$\mathsf{V}_B = \hat{\delta}\ \mathsf{F}, \tag{44c}$$

where N_A is the horizontal force at the point A and V_A and V_B are the vertical components of the resultants at the beam ends A and B, respectively. The parameter $\hat{\delta}$ denotes the ratio $\hat{\delta} = \frac{X_C}{X_B}$, the relative position of the point C.

Now, the internal resultant $\vec{\mathsf{R}}$ can be reach by studying the equilibrium of the region on the left side of actuating point and on the right side. We have

$$\vec{\mathsf{R}}^{\pm} = \begin{cases} \mathsf{R}_x^{\pm} = -\mathsf{P} \\ \mathsf{R}_y^{\pm} = \hat{\delta}^{\pm}\ \mathsf{F} \end{cases} \qquad \text{with} \qquad \begin{cases} \hat{\delta}^{-} = \hat{\delta} - 1, & \forall S \in [0, S_C[\\ \hat{\delta}^{+} = \hat{\delta}, & \forall S \in]S_C, 1] \end{cases} \tag{45}$$

where the subscript $(-)$ refers to the left region while $(+)$ refers to the right one.

3.3.2. Final form of the set of equations of the buckled beam

On using the different equations obtained in the previous subsections and combining Eqns (39, 42) and Eqn. (45), the static equations for the present buckling beam take on the form

$$\begin{cases} \dfrac{d^2\theta}{dS^2} + \hat{\delta}^{\pm}\ \mathsf{F}\cos\theta + \mathsf{P}\sin\theta - k\hat{\delta}^{\pm}\ \mathsf{PF}\cos(2\theta) - \dfrac{1}{2}k[\mathsf{P}^2 - \left(\hat{\delta}^{\pm}\right)^2\ \mathsf{F}^2]\sin(2\theta) = 0, \\ \dfrac{d\vec{Q}}{dS} = \left(1 + k\mathsf{N}^{\pm}\right)\vec{\tau}, \end{cases} \tag{46}$$

the above equations are valid for both segments $[0, S_C[$ and $]S_C, 1]$. The resultant along the beam axis is given by

$$\mathsf{N}^{\pm} = -\mathsf{P}\cos\theta + \hat{\delta}^{\pm}\ \mathsf{F}\sin\theta. \tag{47}$$

3.3.3. Comments

The equations governing the equilibrium of the proposed buckled beam thus obtained deserve some comments and remarks.

1. At a first sight, the extensibility property of the beam produces more or less complicated structure including nonlinear term in the forces F and P. If the beam is inextensible, that is $k = 0$, the bending equation is simplified into a kind of sine-Gordon equation (Drazin , 1983). The latter possesses localized solution in the form of lump structure corresponding to the beam deflexion.
2. The parameter $\hat{\delta}$ denoting the ratio of the abscissa of actuating force to the distance between supports allows us to find an optimal position of the actuating force; which is not necessary located at the beam center.
3. As soon as the bending equation is solved with respect to θ, on using geometric compatibility equations (Eqns (41)) we reach the position $X(S)$ and $Y(S)$ of the buckled beam.

4. Numerical solutions and results

4.1. Numerical method

We start with Eqns (46) and (47). The problem is then to search for the solutions $\theta(S)$, $X(S)$ and $Y(S)$ which must satisfy the boundary conditions on the left end of the beam

$$\left\{\begin{array}{rcl} X(0) & = & 0, \\ Y(0) & = & 0, \\ \theta'(0) & = & 0, \\ \theta(0) & = & \theta_A, \end{array}\right. \tag{48}$$

and on the right end of the beam

$$\left\{\begin{array}{rcl} X(1) & = & X_B, \\ Y(1) & = & 0, \\ \theta'(1) & = & 0, \\ \theta(1) & = & \theta_B, \end{array}\right. \tag{49}$$

In these boundary conditions, θ_A is unknown, X_B is given (it is the end-shortening of the support B), θ_B is unknown, but computed once the solution obtained. Accordingly a numerical shooting algorithm must be used. The input parameters of the method are given by Eqn. (48) and we start with an initial guess for θ_A. The objective parameters are given by Eqn. (49). Nevertheless, we do not know the buckling force P since only the displacement of the right end of the beam is given. Moreover, at each position $Y_C = Y(S_C)$ the vertical coordinate of the applied force corresponds to one deformed beam, while a same actuating force can produce, *a*

priori, different beam deformations. Therefore, the buckling resultant P , the actuating force F and the curvilinear abscissa S_C of the application point are not known. In order to find the so-called shooting parameters θ_A, P, F and S_C we use along with the shooting method a predictor-corrector algorithm starting with initial guess θ_A, P, F and S_C by varying continuously the guessed values until the conditions at the right end of the beam (Eqn. (49)) are fulfilled with a sufficient accuracy. Each solution is recursively found by using a previous one as initial guess for the following step. In the procedure, we use four shooting parameters in order to reach an objective vector with three components. As consequence, an orthogonality condition is required between the predictor vector and corrector one to close the system. Moreover, the orthogonality condition is such that the method convergence is rapidly ensured. The numerical problem concerns the solutions to a set of nonlinear differential equations of two point boundary values problem given by Eqns. (48) and (49) with integral constraint Eqn. (32). The method is based on numerical continuation methods (Allgower and Georg , 2003) which is quite well efficient for the present numerical problem we want to solve.

4.2. Numerical results

4.2.1. Bifurcation diagrams

One of the first results which can be extracted from the numerical computations is the bifurcation diagram. More precisely, the evolution of the buckling load P as function of the end shortening $\Delta\mathsf{L}$ of the elastic beam. In this situation the actuating force F is set to zero. The bifurcation curve shown in Figure 3 exhibits very clearly two domains. As far as the compressive force is less than the critical one, the beam is still straight. The relationship for $\Delta\mathsf{L}$ versus P follows a linear Hook law. Once the applied load is increased by a small amount beyond the critical load, the beam is deformed into a buckled configuration which is just very close to the original straight beam, but with a small transverse deviation. This is the post-buckling regime. The latter increases with the applied load as shown in Figure 3. The insert in Figure 3 shows, in the vicinity of the bifurcation point, the detailed variation of $\Delta\mathsf{L}$ depending on the parameter k.

Influence of the beam extensibility - It is worthwhile examining in details the diagram of bifurcation in the post-buckling regime in the vicinity of the critical load. At this end, we assume small end-shortening and consequently rotations of small amplitudes. We look for solution to the static problem (see Eqn. (46) with no applied transverse force) as a reduced form on the first buckling mode

$$\theta(S) = \theta_0 \cos(\pi S), \tag{50}$$

In order to compute the amplitude θ_0 satisfying the post-buckling regime problem, we expand the Lagrangian of the system Eqn. (43) for small rotations up to the fourth order. We arrive at

$$\tilde{\mathcal{L}} = \int_0^1 [\frac{1}{2}(\theta_{,S})^2 + \mathsf{P}\left(1 - \tfrac{1}{2}kP\right) - \tfrac{1}{2}\mathsf{P}\left(1 - k\mathsf{P}\right)\theta^2 + \tfrac{1}{24}\mathsf{P}\left(1 - 4k\mathsf{P}\right)\theta^4]dS. \tag{51}$$

On considering the first mode solution Eqn. (50) into the new form of the Lagrangian Eqn. (51), after integrating over the segment $[0, 1]$, the latter takes on the form

$$\tilde{\mathcal{L}} = \mathsf{P}\left(1 - \tfrac{1}{2}k\mathsf{P}\right) - \tfrac{1}{4}\left(\mathsf{P} - k\mathsf{P}^2 - \pi^2\right)\theta_0^2 + \tfrac{1}{64}P\left(1 - 4k\mathsf{P}\right)\theta_0^4. \tag{52}$$

which is merely a polynomial function of the fourth order in θ_0. Now, the problem is to find θ_0 which minimizes the Lagrangian Eqn. (52). The necessary condition reads as $\frac{\partial\tilde{\mathcal{L}}}{\partial\theta_0} = 0$, yielding

$$\theta_0[\mathsf{P}\left(1 - k\mathsf{P}\right) - \pi^2 - \tfrac{1}{8}\mathsf{P}\left(1 - 4k\mathsf{P}\right)\theta_0^2] = 0. \tag{53}$$

It can be checked that the trivial solution $\theta_0 = 0$ (straight beam) corresponds to a maximum of the Lagrangian (unstable solution), while the solution $\theta_0 \neq 0$ realizes the minimum. We find

$$\theta_0^2 = \frac{8}{\mathsf{P}}\left[\frac{\mathsf{P}\left(1 - k\mathsf{P}\right) - \pi^2}{1 - 4k\mathsf{P}}\right]. \tag{54}$$

For inextensible beam ($k = 0$) and $\mathsf{P} \geq \pi^2$ (post-buckling regime), we recover the classical formula $\theta_0 = \pm 2\sqrt{\frac{2}{\mathsf{P}}\left(\mathsf{P} - \pi^2\right)}$. From Eqn. (54), the rotation amplitude θ_0 becomes non zero for a critical load slightly greater than π^2 because of the beam compressibility. We can say that for small k, the critical loading can be approximated by $\mathsf{P}_c \simeq \pi^2\left(1 + k\pi^2\right)$. We can observe on the diagram of bifurcation the tiny shift of the critical load relative to the inextensibility theory. This is why the extensibility hypothesis of the beam becomes significant as soon as we deal with small end-shortening and rotations or displacements of small amplitudes. On the bifurcation diagram, Figure 4, the curve of θ_0 as function of loading force P (see Eqn. (54)), has been superposed to the solution coming from the numerics. The difference is not practically observable.

4.2.2. Elastic beam response under actuating force

Now, we introduce the action of an applied transverse force F. In this section we want to determine the actuating force as function of the vertical displacement of the mid-point of the beam for given end-shortening $\Delta\mathsf{L}$ and compressibility parameter k.

The first numerical results deal with the central actuating and the force is maintained vertically at the abscissa X_C such that $\hat{\delta} = 0.5$. The vertical displacement of the actuating force $Y_C = Y(S_C)$ at the point C is controlled step by step. The corresponding actuating force is computed with the help of the numerical algorithm. The force-displacement diagram is shown in Figure 5. A classical N-shaped curve is obtained. Such results can be compared to those presented by different authors (Vangbo , 1998; Qiu et al. , 2004) using different approaches, essentially based on buckling mode expansion. More precisely, there are several branches on the graph. The first branch starts at the either both stable positions (point a_1 or a_2 on Figure 5). The crossing point of the branch involving the first buckling mode and that for the second mode

occurs for the bifurcation actuating force $\mathsf{F} = \mathsf{F}_b$ at the point b_1. On decreasing the actuating force the branch $(b_1 b_2)$ passes through the point c_1 corresponding to $Y_C = 0$ with $\mathsf{F} = 0$. The curve is symmetric with respect to the origin. It is worthwhile noting that the slope of the $\mathsf{F} - Y_C$ diagram is negative, this means that the bistable system possesses a negative stiffness on this branch. Because of the symmetry of the structure, two symmetric solution exist for the second buckling mode, but these solutions share the same branch $(b_1 b_2)$. The branch selection is ensured by an energetic criterium. The part of the graph drawn in dashed line represents the non-admissible path, that is, the path with greater energy. In addition the branch is unstable, because the snap-through of the beam involves a zero mode (straight beam). Quite similar results have been obtained by (Pi. , 2007) for circular shallow arches subjected to uniform loading and simply supported.

Figure 6 shows the non dimensional compressive force P as function of the vertical coordinate Y_C of the point C. We can observe that as far as $\mathsf{P} \geqslant 4\pi^2$, the snap-through from one stable state to the other one occurs involving a buckling mode 2. The upper branch corresponds to a greater energy. The corresponding points introduced for the force-displacement diagram have been reported in the $\mathsf{P} - Y_C$ curve. We have the bifurcation points b_1 and b_2 for which the lower branch $(b_1 c_1 b_2)$ corresponds to the second buckling mode.
Instructive details are given by the graph of the total energy $\mathcal{E}_{tot}$ of the bistable system as function of the vertical coordinate Y_C shown in Figure 7 for the central actuation and for an end-shortening of 3 %. The two minima of the energy are located at the stable positions either the downwards buckling beam (point a_1) or the upwards one (point a_2) for null actuating force. At the bifurcation points b_1 and b_2 the energy graph splits into two branches the lower one for the admissible solution and upper one for the non-admissible solution.

A second series of numerical results is obtained for shifted actuating force (force not applied to the beam center). In this situation we want to examine the influence of the position of the actuating force in the bistable system response. Especially, the question is, is there an optimal position? In the work of Cazottes et al. (Cazottes et al. , 2010) the advantage of shifted actuating force is experimentally placed in evidence. In particular, this mode of actuation needs a maximum of the actuating force smaller than that of the central actuation for a given end-shortening. We perform numerical simulation by varying the ratio $\hat{\delta}$ (or the location of the actuating force) for an end-shortening of about 3 %. Figure 8 presents the maximum of actuating force as function of the ratio $\hat{\delta}$. The graph exhibits clearly two symmetric minima. The first minimum is located at 39 % of the total length of the beam.
We consider the actuating force located at the optimal position and we observe the displacement of the beam center (at $S = 0.5$). The result is then drawn in Figure 9 with a graph possessing three loops. The curve in solid line corresponds to admissible solution (path $(a_1 b_1 c_1 d_1 b_2 a_2)$) and (path $(a_2 b_2 c_2 d_2 b_1 a_1)$) while the one in dashed-line is for higher actuation energy. The crossing

point of the branch using the first buckling mode and that of the second mode is referred as to b_1. The two symmetric points c_1 and c_2 correspond to $\mathsf{F} = 0$ and those noted d_1 and d_2 are for $Y_C = 0$. Because of the dissymmetric loading the path going from the upwards solution (point a_2) to the downwards position (point a_1) is different from the path for the inverse switching.
The buckling force P which imposes the end-shortening fixed is plotted in Figure 10 as function of the displacement Y_C. The different points defined on Figure 9 have been reported on the $\mathsf{P} - Y_C$ diagram. In particular, the points d_1 and d_2 for $Y_C = 0$ have the same locus. The total energy $\mathcal{E}_{tot}$ of the bistable system versus Y_C is presented in Figure 11. Similarly as for the central actuation, the curve exhibits two branches, the lower branch corresponds to the admissible path for the actuating response of the bistable beam. It is worthwhile observing that even if we have two branches for the admissible solution. As matter of fact, the branch $(b_1 d_1 b_2)$ and the branch $(b_1 d_2 b_2)$ share the same part of curve in the $\mathcal{E}_{tot} - Y_C$ diagram. It means physically that the switching from upwards buckling position to the downwards one and the reverse switching need the same energy.

4.2.3. Influence of the end-shortening on bistable beam response under actuating force

The model of the bistable buckled beam possesses, in its dimensionless representation, two important parameters : (i) the end-shortening of the right end of the beam $\Delta\mathsf{L}$ (parameter of configuration) and (ii) the extensibility parameter k which depends mainly on the slenderness ratio of the beam (geometric parameter). The other parameters are controlling quantities, especially, the buckling force P is subject to the limit condition at $S = 1$, such that $X(1) = X_B$ which is given (see Eqn. (31) or Eqn. (49)).
In this subsection we want to know how the end-shortening $\Delta\mathsf{L}$ modifies the response of the bistable beam, that is, the paths of the actuating force as function of its vertical position on the beam. The response to this question is illustrated in Figure 12 for four typical values of the end-shortening and for central actuation. We observe that the number of branches for the curve F versus Y_C increases as $\Delta\mathsf{L}$. This means that physically for a given Y_C the number of equilibrium solutions to the static equations becomes more numerous. This does not means that all the solutions are stables. Only, the one corresponding to the lowest energy is the admissible solution.

4.2.4. Influence of the extensibility parameter on bistable beam response under actuating force

For a given end-shortening ($\Delta\mathsf{L} = 0.03$), the extensibility parameter k (see Eqn. (38) for definition) is varied. Figure 13 represents three situations corresponding to three values of k ($k = \frac{1}{20000}$, $k = \frac{1}{5000}$ and $k = \frac{1}{2500}$). We observe that the number of branches of the $F - Y_C$ diagram for equilibrium solutions is more numerous as k is getting smaller, which is physically reasonable since the beam is more flexible leading to a great number of equilibrium configurations for a given actuating force. For k rather moderate the number of branches remains limited to a couple of branches. In fact, the extensibility parameter k represents the ratio of the compressive beam energy to the bending energy, physically, that means that the

bending energy is more important for k small or for slender beams. As consequence, for different values of the actuating force F correspond to different levels of energy. Only the lowest level of energy leads to the stable equilibrium solution. In order to compare the influence of the extensibility on the $F - Y_C$ diagram, the graphs on Figure 13 are plotted in dimension unit for the force. The actuating force at the bifurcation point b_1 of the $F - Y_C$ diagram have been computed, we find F_b. The actuating force at the bifurcation point b_1 of the $F - Y_C$ diagram have been computed, we have $F_b = 4651.85\ N$, $F_b = 2834.82\ N$ and $F_b = 784.77\ N$ respectively for $k = \frac{1}{2500}$ ($\frac{L}{h} = 14.43$), $k = \frac{1}{5000}$ ($\frac{L}{h} = 20.41$) and $k = \frac{1}{20000}$ ($\frac{L}{h} = 41$). In the case of an inextensible beam ($k = 0$) the corresponding forces take on the following values $F_b = 6446.95\ N$ ($-38.6\,\%$), $F_b = 3223.47\ N$ ($-13.5\,\%$) and $F_b = 805.87\ N$ ($-2.7\,\%$). An extra comparison can be done with a very small $k = 3 \times 10^{-7}$ ($\frac{L}{h} = 500$ very slender beam), $F_b = 4.837\ N$ to be compared to $F_b = 4.835\ N$ ($0.04\,\%$) obtained with $k = 0$. The percentages represent the difference between inextensible model with respect to extensible one.

4.3. Analysis of the role of buckling modes in the bistable snap-through

4.3.1. Reduced model

In this part we want to show how the bistable system uses the buckling modes for the switching process from one stable state to the other one. In Section 4.2.1, it has been examined the bifurcation diagram in the post-buckling regime for moderate rotation. Accordingly, it is reasonable to investigate the post-buckling behavior of the system using reduced order model. We consider a finite-dimensional approximation of the solution to the beam equations by expanding the rotation $\theta(S)$ as a series of buckling modes truncated at the Kth order

$$\theta(S) = \sum_{j=1}^{K} A_j \cos(j\pi S), \tag{55}$$

where the A_j's are the amplitude associated to the jth mode. The approximation Eqn. (55) can be viewed as a truncated Fourier series. The Fourier coefficient being A_j and they can be computed by using the orthogonality properties of the buckling modes, thus we have

$$A_j = 2\int_0^1 \theta(S)\cos(j\pi S)\, dS. \tag{56}$$

Now, for each value Y_C of the vertical position of the actuating force F we compute the admissible solution $\theta(S)$ with Y_C as parameter. On considering Eqn. (56) , the coefficient A_j depend only on Y_C, all other ones are completely determined for a given end-shortening. The first three coefficients A_j ($j = 1, 2, 3$) are plotted in Figure 14 versus Y_C. It is clear that, in practice and during the switching process the first two buckling modes are predominant. The third mode even if it is not null, it remains rather small in comparison to the other two.

Here and henceforth, the analysis is done in hypothesis of moderate rotation. Then we assume a two degrees of freedom model by setting

$$\theta(S) = A_1 \cos(\pi S) + A_2 \cos(2\pi S), \tag{57}$$

Now, the discussion continues with the Lagrangian functional of the bistable system computed with expansion given by Eqn. (57). This functional is now a function of the mode amplitudes A_1 and A_2. We set $\mathcal{L}^{(r)}(A_1, A_2)$ the Lagrangian functional associated with the model reduced to the first two buckling modes using Eqn. (43).

4.3.2. Equilibrium and stability

The equilibrium configurations are defined as the solutions of

$$\frac{\partial \mathcal{L}^{(r)}(A_1, A_2)}{\partial A_j} = 0, \qquad \text{for} \quad j = 1, 2. \tag{58}$$

The stability of the equilibria is examined by the Dirichlet theorem for potential system (Thompson and Hunt , 1973; Huseyin , 1986; Quoc Son , 1995), that is, the 2×2 Hessian matrix of $\mathcal{L}^{(r)}$ is

$$H_{ij}(A_1, A_2) = \frac{\partial^2 \mathcal{L}^{(r)}(A_1, A_2)}{\partial A_i \partial A_j}, \qquad \text{for} \quad i, j = 1, 2. \tag{59}$$

If the matrix H is positive definite, i.e., if all the eigenvalues of H are positive, the system is stable, because the Lagrangian functional is convex. If one or more eigenvalues are negative the system is unstable, because the Lagrangian functional is concave with respect to one or two directions determined by the associated eigenspaces.

The Lagrangian functional of the system is a function of the amplitudes A_1 and A_2 and P as well, the buckling force. The latter depends on the equilibrium configuration for a given end-shortening. This dependency is given by Eqn. (31) or Eqn. (32) which can be written as

$$X(1) = X_B = \int_0^1 X'(S) dS = \int_0^1 [1 - k\mathsf{P} \cos(\theta(S))] \cos(\theta(S)) \, dS. \tag{60}$$

where $\theta(S)$ is given by Eqn. (57). Eqn. (60) allows us to compute the buckling force P as function of the amplitudes A_1 and A_2 for a given end-shortening. Now, the Lagrangian functional can be plotted in the (A_1, A_2)-plane. Figure 15 shows the 3D graph of the Lagrangian functional as function of A_1 and A_2. The graph exhibits an unstable equilibrium configuration for $A_1 = A_2 = 0$. But, for $A_2 = 0$ there exists two stable configurations for $A_1 = A_{10} \neq 0$, where A_{10} is the amplitude of the first buckling mode with null actuating force. It corresponds to the first buckling mode (upwards for $A_{10} > 0$ and downwards otherwise) when the actuating force is not applied. The surface possesses two saddle points for $A_1 = 0$ and $A_2 \neq 0$ which means that the Lagrangian functional is convex in the A_2-direction while it is concave in A_1-direction as shown in Figure 15.

According to the study of the bistable response for actuating force as function of the vertical

position Y_C, we are able to parameterize the switching path going from one stable position to the other one and vice versa in the contourplot graph in the (A_1, A_2)-plane. Figure 16 shows such contourplot where the closed curve marks the limit of the unstable region. The latter is determined by examining the sign of the eigenvalues of the Hessian matrix Eqn. (59). For each position Y_C while the bistable moves quasi-statically, there exists an equilibrium corresponding to an unique actuating force as examined in Section 4.2.2. Two kinds of numerical results are reported. The first result deals with a central force actuation. The path (P_1) is the result, it is obtained by controlling the switching from the stable position $(A_{10}, 0)$ to the other one $(-A_{10}, 0)$ for each value of the vertical position Y_C. The equilibrium positions are computed leading to the solution $(A_1(Y_C), A_2(Y_C))$. The path (P_1) starts using mainly a first buckling mode in the stable region and it quickly enters the instability domain. The second buckling mode increases at the cost of the first mode passing through the saddle point of the domain. A second result is presented - path (P_2) - for non central force at 40% from the left end $(\hat{\delta} = 0.4)$. In this situation, the beam begins to switch using a non zero amount of the second buckling mode. The equilibrium path (P_2) enters the instability region passing through by the saddle points $(0, \pm A_{20})$ as the path (P_1). The bistable beam follows the path (P_1) or (P_2) using the control of the actuating force quasi-statically until the intersection point with the instability region is reached. Beyond this point the bistable system becomes unstable and jumps to the other stable position by making use of the second buckling mode which is the less energetic mode as already presented for the actuation force response. It is worthwhile noting that while the bistable beam switching whatever the actuating force position the energy barrier to be overtaken is the same. Nevertheless, a non-central actuation allows to delay the bistable system entering the instability domain. Similar instability phenomena can be met for shallow arches where the switching process depends on the arch height (Vangbo , 1998; Qiu et al. , 2004; Cen and Lin , 2005).

5. Comments and concluding remarks

The main objects of the proposed work are twofolds. The first goal is to report a model for bistable buckled beam based on elastica theory including extensibility. On using the complete model we next examine, in details, the switching process of the bistable mechanism. The second goal deals with numerical results among them the bistable response to localized actuating force according to the application position on the beam and switching scenarios. The present analysis based on an extensible elastic beam reveals interesting buckling mode contributions to the snapping effect by applying a punctual force and controlling the displacement of the vertical position of the actuating force. The governing beam equations for large-displacement and finite-strain hypotheses have been deduced from a correct variational formulation based on the virtual work principle under the Euler-Bernoulli beam kinematics.

The most pertinent results describing the behavior of the bistable buckled beam are obtained

by using a numerical algorithm based on continuation scheme and Newton-Raphson method. This apparently more or less simple bistable structure is rich enough to provide particularly interesting results :

- The role played by extensibility parameter k in the post-buckling regime has been put in evidence for the bifurcation diagram analysis. It is interesting to note that for small end-shortenings of the beam and in the post-buckling regime, the beam extensibility becomes appreciable.

- Important results concern the response of the bistable system to the action of a transversally localized force. For a given Y_C - the vertical position of the actuating force - there exist several branches of solution to the static problem. Nevertheless, only one solution is really admissible. The branch selection has been done using an energetic criterium, the solution corresponding to the lowest energy is possible. Two kinds of results have been obtained (i) for central actuation ($\hat{\delta} = 0.5$) and (ii) for shifted force actuation ($\hat{\delta} = 0.39$). In each situation the response of the bistable buckled beam is different according to the parameter k (extensibility parameter) and the end-shortening $\Delta\mathsf{L}$. Especially, the number of branches of solution increases while k is getting smaller and $\Delta\mathsf{L}$ increases as well.

- The numerical simulations are performed for the end-shortening $\Delta\mathsf{L}$ maintained fixed while the bistable switches, this means that the buckling loading depends on the vertical position of the actuating force. Accordingly, the relation between the buckling force and the position Y_C has been computed for both situations central and shifted actuations. The results are illustrated in Figures 6 and 9.

- In the framework of the reduced model (two degrees-of-freedom model), the transition from stable equilibrium position to the other one follows equilibrium path passing through the unstable region of the bistable energy. The switching scenarios involve both first and second buckling modes. More precisely, the buckled beam starts switching using the first buckling mode and very quickly the second mode increases at the cost of the first mode. At this stage the switching process is largely dominated by the second buckling mode. The process is then reversed when the bistable buckled beam goes out of the unstable domain to reach the other stable position.

- An optimal position of the actuating force has been placed in evidence. For an actuation localized at about 39 % from the left or the right of the beam we have the minimum actuating force. This result was already pointed out by Cazottes et al. (Cazottes et al. , 2010), but on using another approach. These results can be of relevant interest for engineering applications such as micro-switches or MEMS.

A natural extension of the present work would be comparisons of the present numerical results to experimental tests in order to validate the proposed model based on the elastica beam

theory. Experimental identifications of the bistable buckled beam are in progress and will be proposed in future works. Moreover, one of the most interesting studies would be the dynamical response of the bistable system under time dependent excitations, the latter extension will be also explored in forthcoming researches.

References

Allgower E.G., Georg K. : Introduction to numerical continuation methods (SIAM, Philadelphia, 2003).

Baker M.S., Howell L.L., On-chip actuation of an in-plane compliant bistable micromechanism. J. Microelectromechanical Systems 11, 560-573 (2002).

Benali-Khoudja M., Hafez M., Kheddar A., Vital : An electromagnetic integrated tactiles display. Display 28, 133-144 (2007).

Brenner M.P., Lang J., Li J., Qiu J., Slocum A., Optimal design of a bistable switch. Proc. Natl Acad Sci. 100, 9663-9667 (2003).

Buchaillot L., Millet O., Quevy E., Collard D., Post-buckling dynamic behavior of self-assembled 3D microstructures. Microsyst. Technol. 14, 69-78 (2008).

Cazottes P., Fernandes A., Pouget J., Hafez M., Bistable buckled beam : Modeling of actuating force and experimental validations. ASME J. Mech. Design 131, 1001001-1001011 (2010)

Cen J.S., Lin J.S., Exact critical loads for a pinned half-sine arch under end couples. ASME Journal of Applied Mech. 72, 147-148 (2005).

Drazin P.G. : Solitons (Cambridge University Press, Cambridge, 1983).

Eringen A.C., Mechanics of Continua (John Wiley & Sons, 1967).

Fang W., Wickert J.A., Postbuckling of micromachined beams. J. Micromech. Microeng. 4, 118-122 (1994).

Hafez M. : Tactile interfaces : technologies, applications and challenges. Visual Comput. 23, 267-272 (2007).

Hummer A., Irschik H., Large deformation and stability of an extensible elastic with an unknown length. Int. J. Solids and Structures 48, 1301-1310 (2011).

Huseyin K., Multiple parameter stability theory and its applications (Oxford University Press, Oxford, 1986).

Irschik H., Gerstmayr J., A continuum mechanics based derivation of Reissner's large-displacement finite-strain beam theory : the case of plane deformations of originally straight Bernoulli-Euler beams. Acta Mech. 206, 1-21 (2009).

Jensen B.D., Howell L.L., Salmon L.G., Design of two-link, in-plane, bistable compliant micro-mechanism. J. Mech. Design. Trans. ASME 121, 416-419 (1999).

Krylov S., Dick N., Dynamic stability of electrostatically actuated initially curved shallow micro-beams. Continuum Mech. Thermodyn. 22, 445-468 (2010).

Krylov S., Ilic B., Lulinsky S., Bistability of curved microbeams actuated by friging electrostatic fields. Nonlinear Dynamics 66, 403-426 (2001).

Magnusson A., Ristinmaa M., Ljung C., Behaviour of the extensible elastica solution. Int. J. Solids and Struct. 38, 8441-8457 (2001).

McInnes C.R., Waters T.J., Reconfiguring smart structures using plane space connections. Smart. Mater. Struct.17, 025030 (2008).

Nayfeh H., Enam S.A., Exact solution and stability of post-buckling configurations of beams. Nonlinear Dynamics 54, 395-408 (2008).

Patricio P., Adda-Bedia M., Ben-Amar M., An elastica problem : instabilities of an elastic arch. Physica D 124, 285-295 (1998).

Pinto O.C., Gonçalves P.B., Active non-linear controm of buckling and vibrations of a flexible buckled beam. Chaos Solitons & Fractals. 14, 227-239 (2002).

Pippard A.B. : The elastic arch and its modes of instability. Eur. J. Phys. 11, 359-365 (1990).

Pucheta M. A., Cardona A., Design of bistable compliant mechanisms using precision-position and rigid-body replacement methods. Mechanism and Machine Theory 45, 304-326 (2010).

Qiu J., Lang J.H., Slocum A.H., A curved-beam bistable mechanism. J. Microelectromechanical Syst. 13, 134-146 (2004).

Pi Y.-L., Bradford M.A., Tin-Loi F., Nonlinear analysis and buckling of elastically supported circular shallow arches. Int. J. Solids and Structures 44, 2401-2425 (2007).

Quoc Son N., Stabilité des structures élastiques (Springer-Verlag, Berlin, 1995).

Reissner E., One-dimensional finite-strain beam theory. The plane problem. Z. Angew. Math. Phys (ZAMP) 23, 795-804 (1972).

Reissner E., On a one-dimensional large-displacement finite-strain beam theory. Stud. Appl. Math. 52, 87-95 (1973).

Reni H., Gerhard E., Design and fabrication of a current-pulse-excited bistable magnetic microactuator. Sensors and Actuators A Physical 58, 259-264 (1997).

Saif M.T.A., On a tunable bistable NEMS - Theory and experiments. J. Microelectromechanical System 9, 157-170 (2000).

Schomburg W.K., Groll C., Design optimization of bistable microdiaphragm valves. Sensors and Actuators A64, 259-264 (1998).

Simo J.C., A finite strain beam formulation. The three-dimensional dynamics problem. Part I. Comp. Meth. Appl. Mech. Eng. 49, 55-70 (1985).

Taher M., Saif A., On a tunable bistable MEMS - Theory and experiment. J. Microelectromechanical Syst. 9,151-170 (2000).

Thompson J.M.T., Hunt G.W., A general theory of elastic stability (John Wilet & Sons, London, 1973).

Vangbo M., An analytical analysis of a compressed bistable buckled beam. Sensors and Actuators A69, 212-216 (1998).

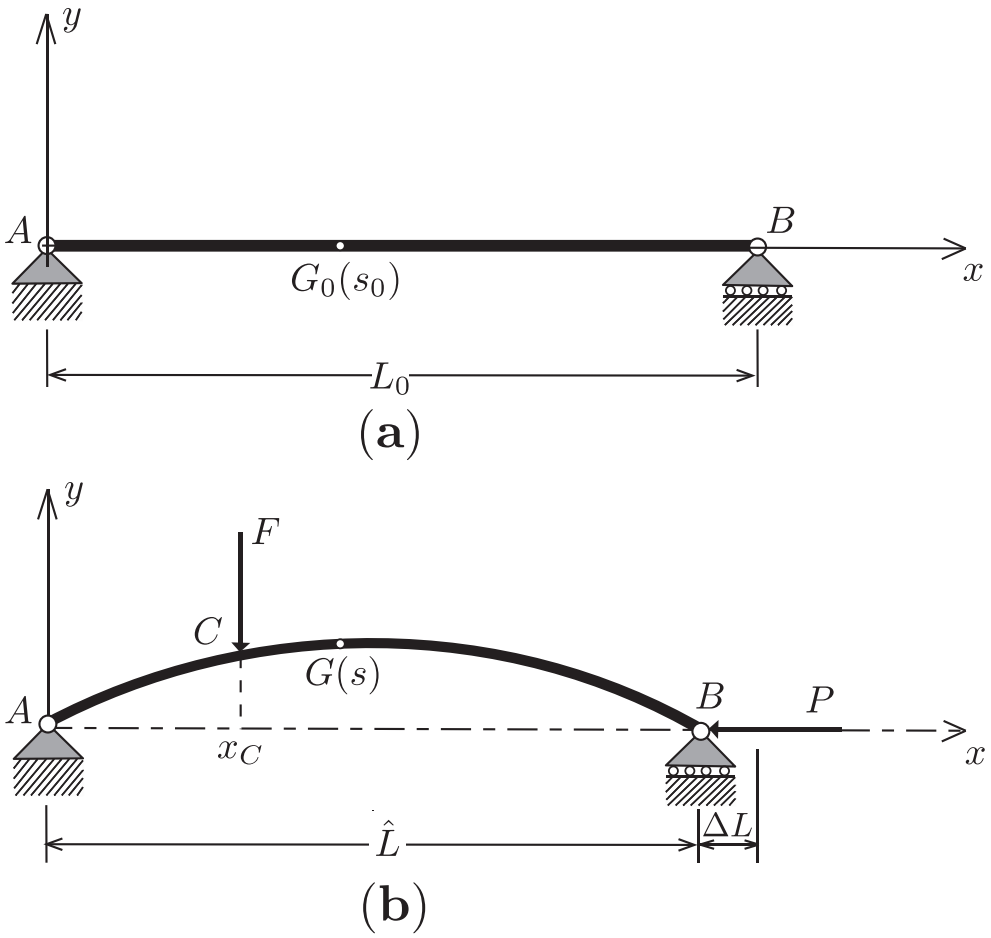

Figure 1: Elastic beam simply supported : (a) the non loaded beam, (b) beam in its buckled configuration with the actuating force.

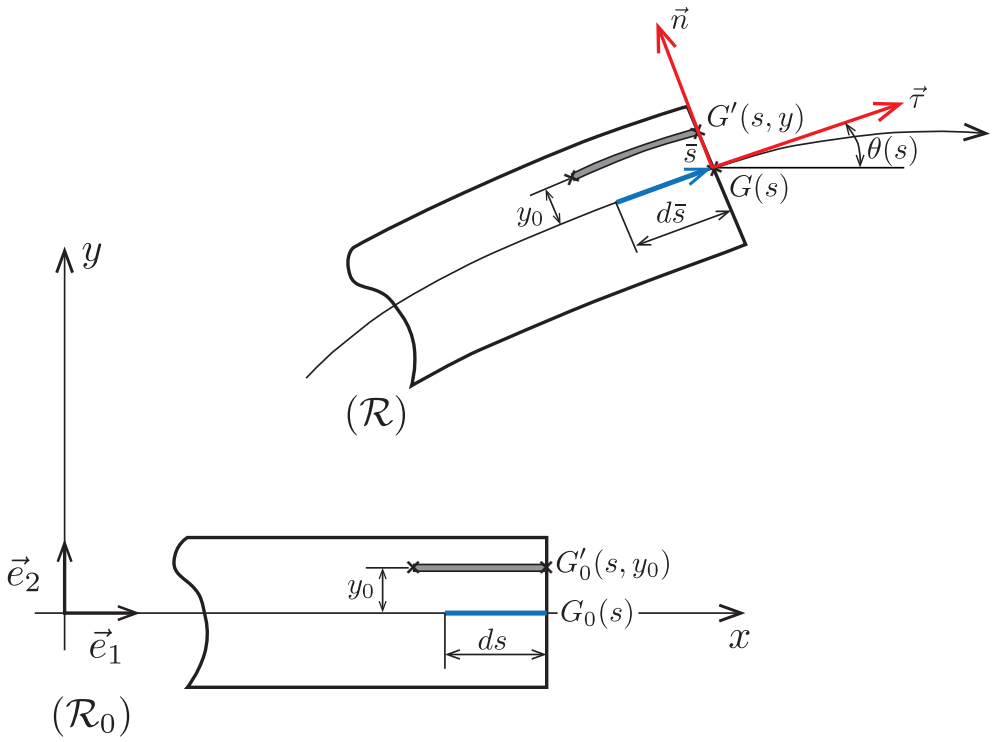

Figure 2: Reference configuration (underformed state) $\mathcal{R}_0$ and current configuration $\mathcal{R}$ (deformed state) with the parameters of the beam configuration.

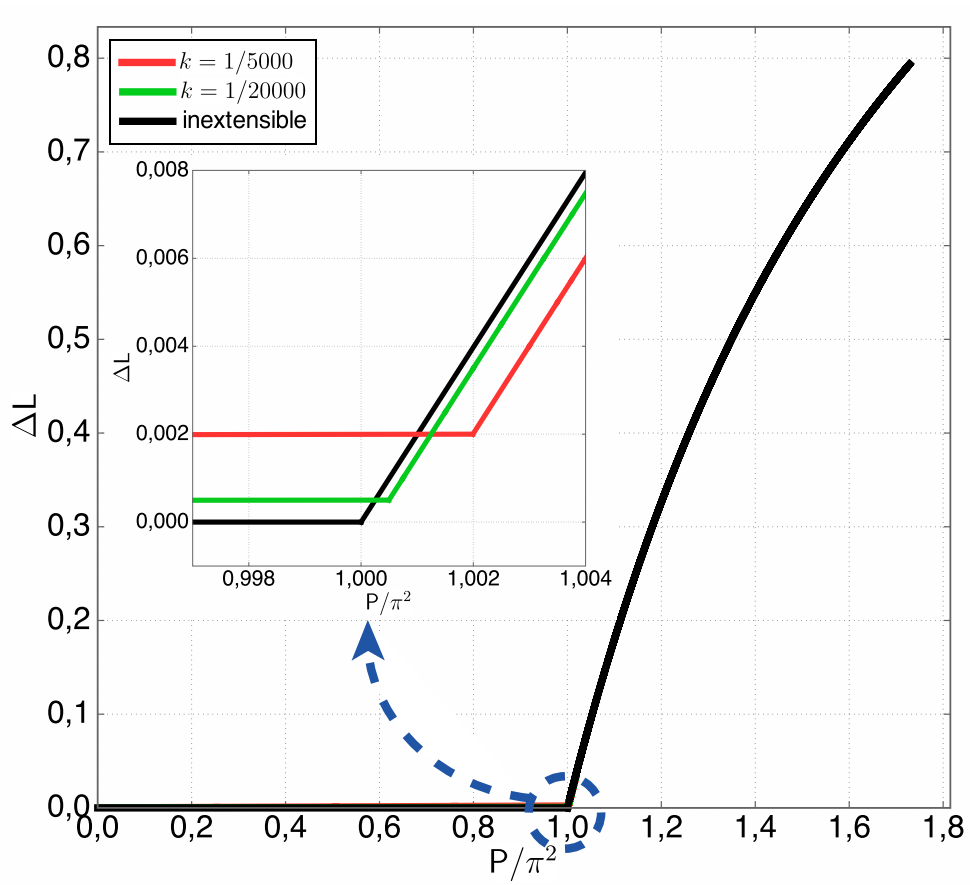

Figure 3: Bifurcation diagram : the end-shortening $\Delta\mathsf{L}$ v.s. the buckling force P (for $k = 1/5000$, $k = 1/20000$ and $k = 0$). The inset shows the details around the critical force and comparison to inextensible beam.

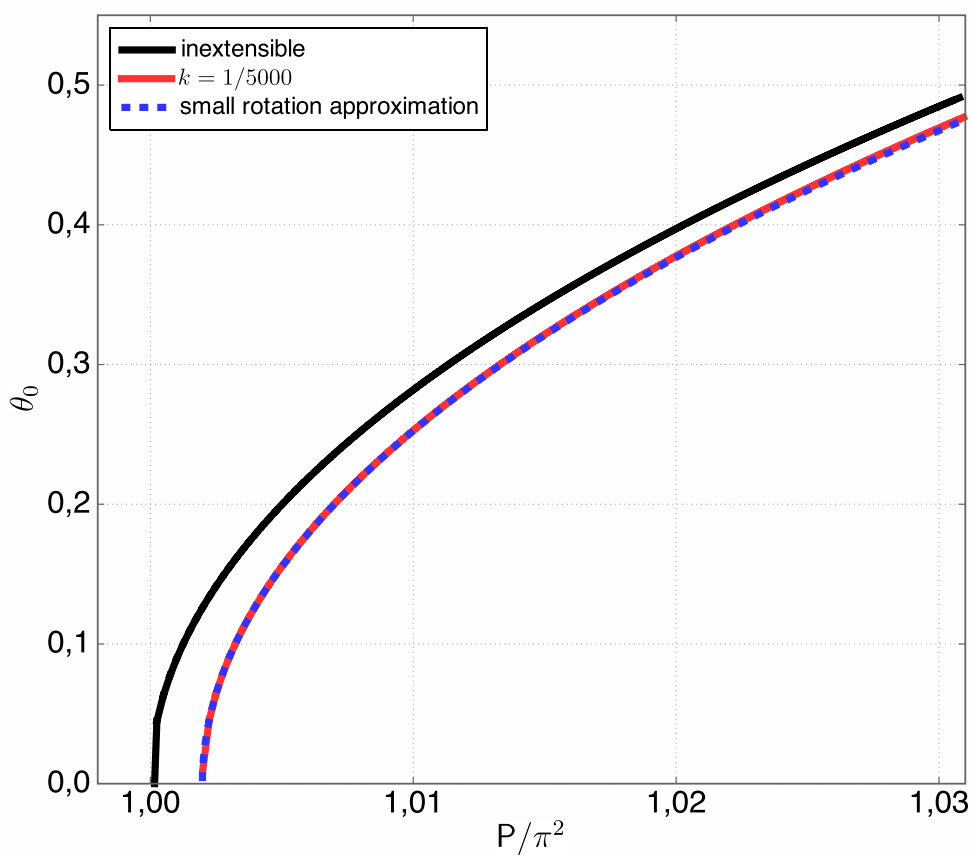

Figure 4: Bifurcation diagram : the rotation amplitude θ_0 as function of the buckling force. Comparison to the inextensible elastica and comparison to the moderate rotation approximation nearby the critical buckling force.

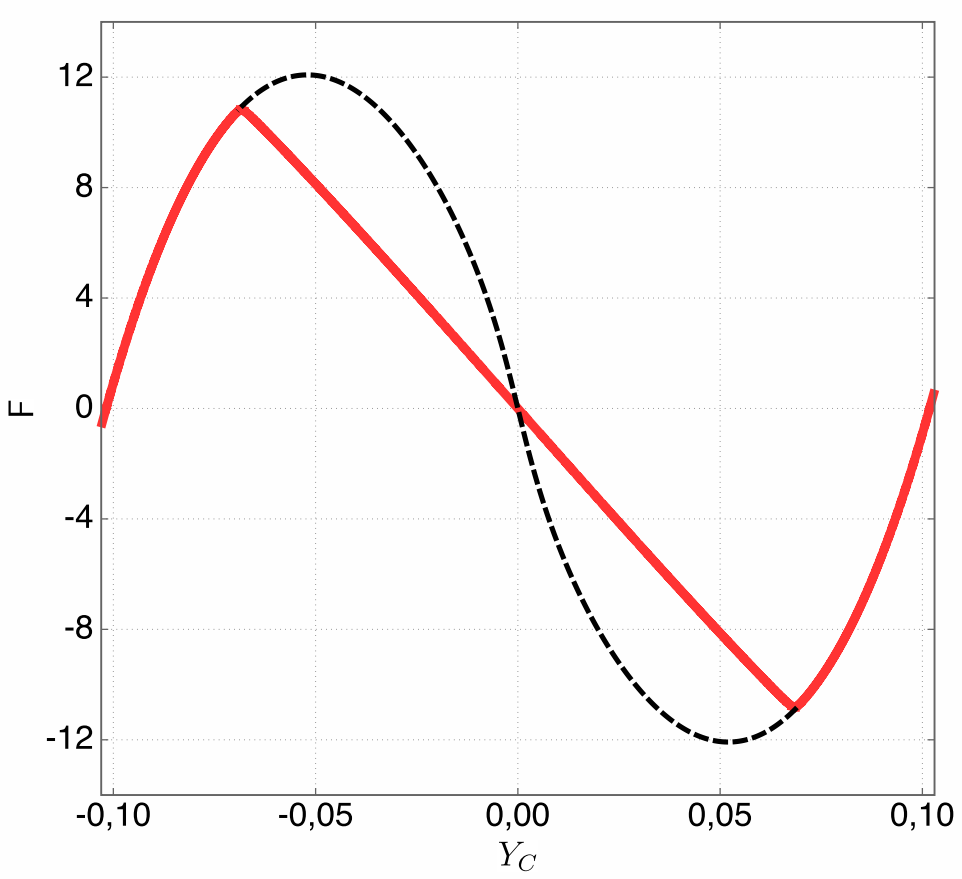

Figure 5: Response of the bistable beam for central actuating force v.s. the vertical position Y_C (for $k = 1/2500$ and $\Delta \mathsf{L} = 0.03$).

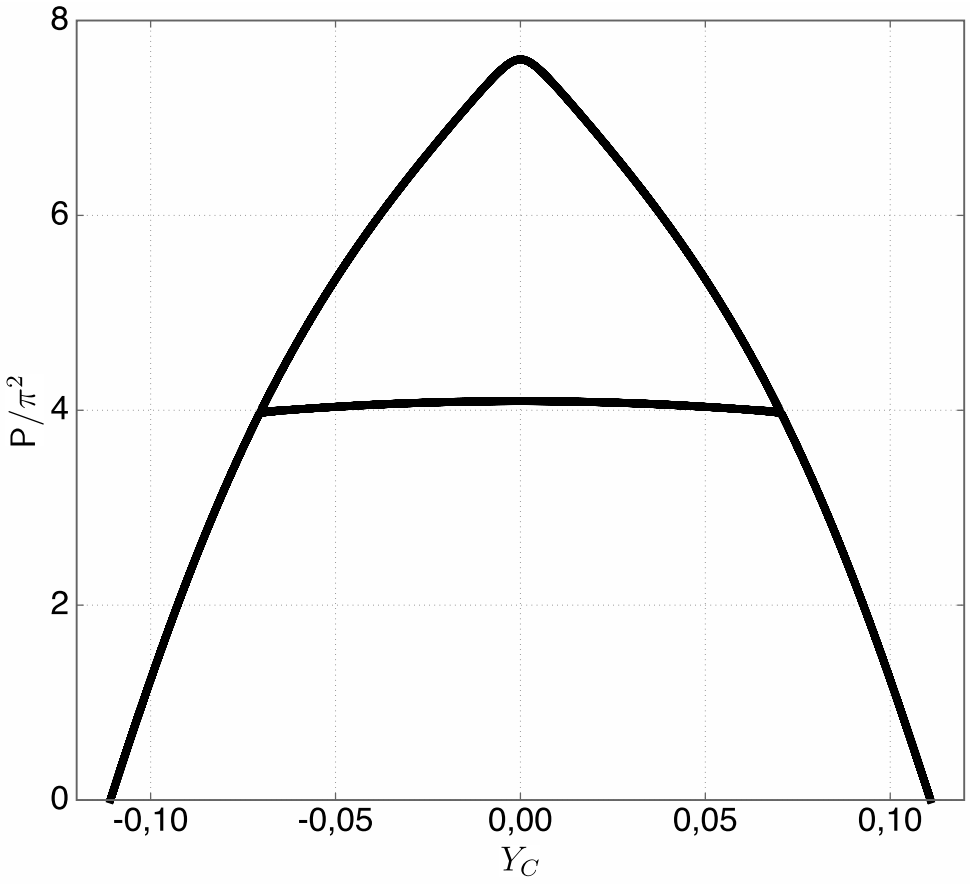

Figure 6: The buckling force as function of the position Y_C in the case of central force actuation. The lower branch is that of associated with the admissible solution (for $k = 1/2500$ and $\Delta\mathsf{L} = 0.03$).

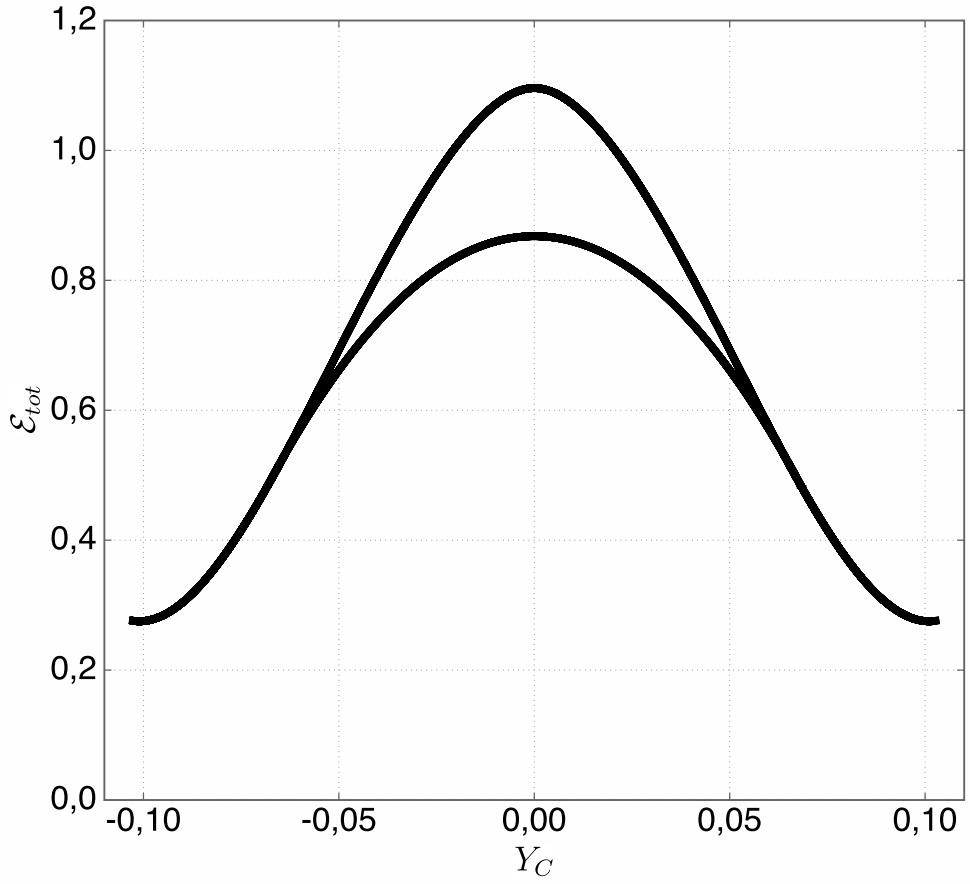

Figure 7: The total energy as function of the position Y_C in the case of central force actuation. Two branches are present. The admissible solution corresponds to the lowest energy (for $k = 1/2500$ and $\Delta\mathsf{L} = 0.03$).

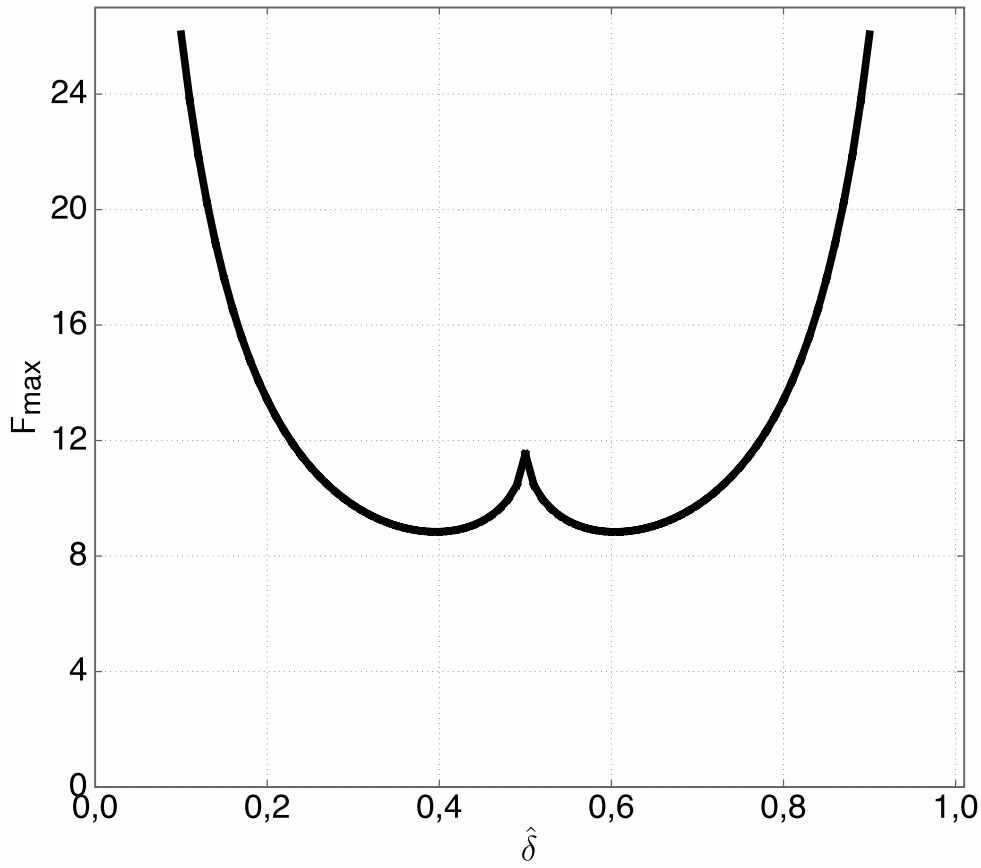

Figure 8: The influence of the actuating force position on the maximum of the applied force (for $k = 1/2500$ and $\Delta\mathsf{L} = 0.03$).

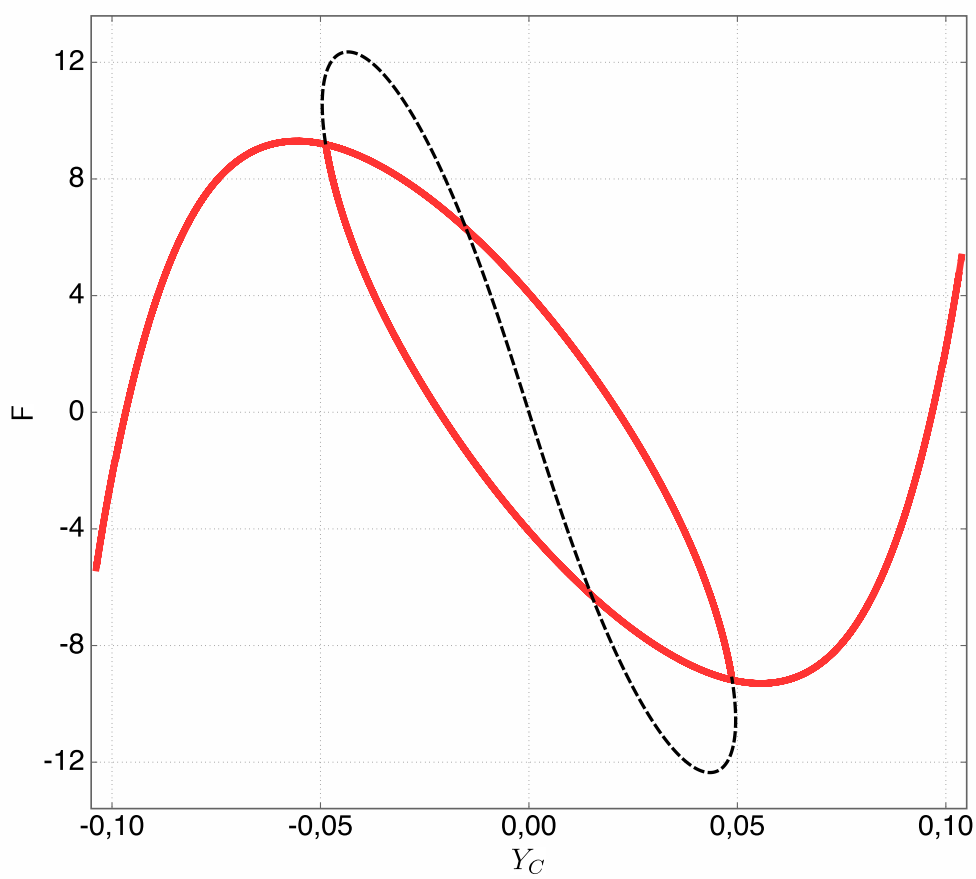

Figure 9: Graph for the shifted actuating force (at 39 %) as function of the its vertical position Y_C (for $k = 1/2500$ and $\Delta\mathsf{L} = 0.03$). The graph possesses several branches of solution to the static problem. Only the branches in solid line correspond to the admissible solution while the one in dashed-line is for higher total energy.

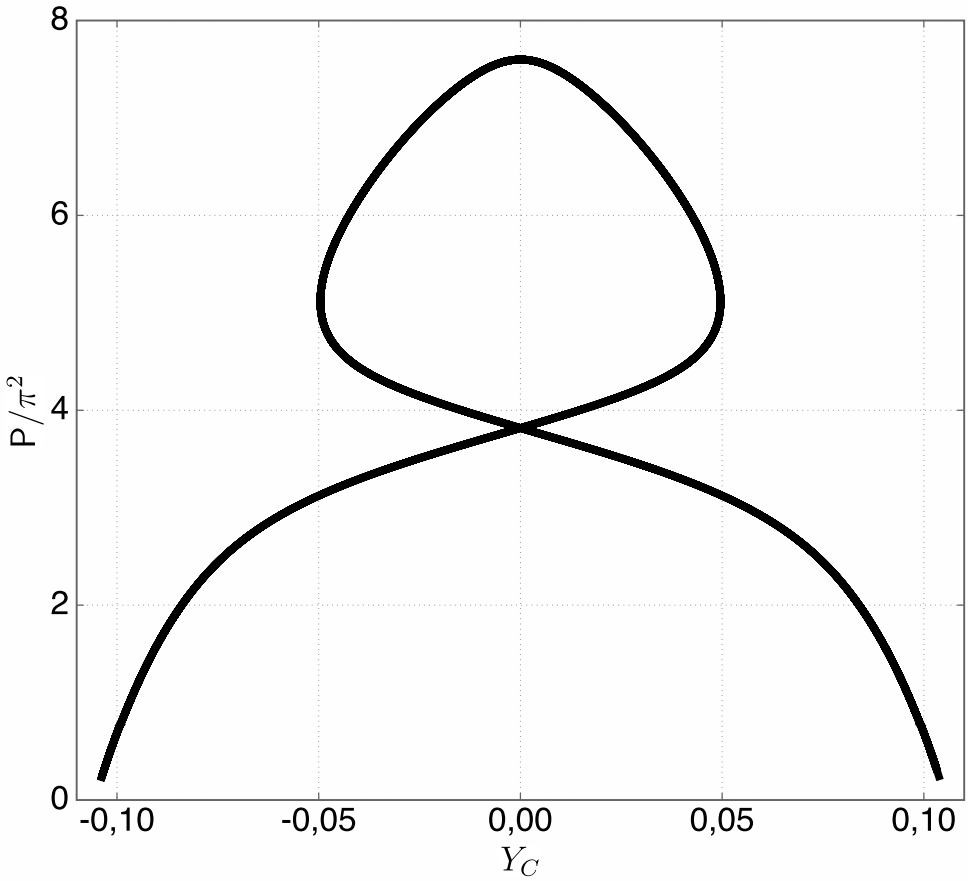

Figure 10: The buckling force as function of the position Y_C for a non-central actuation (at 39 %). The lowest branch corresponds to the admissible solution (for $k = 1/2500$ and $\Delta\mathsf{L} = 0.03$).

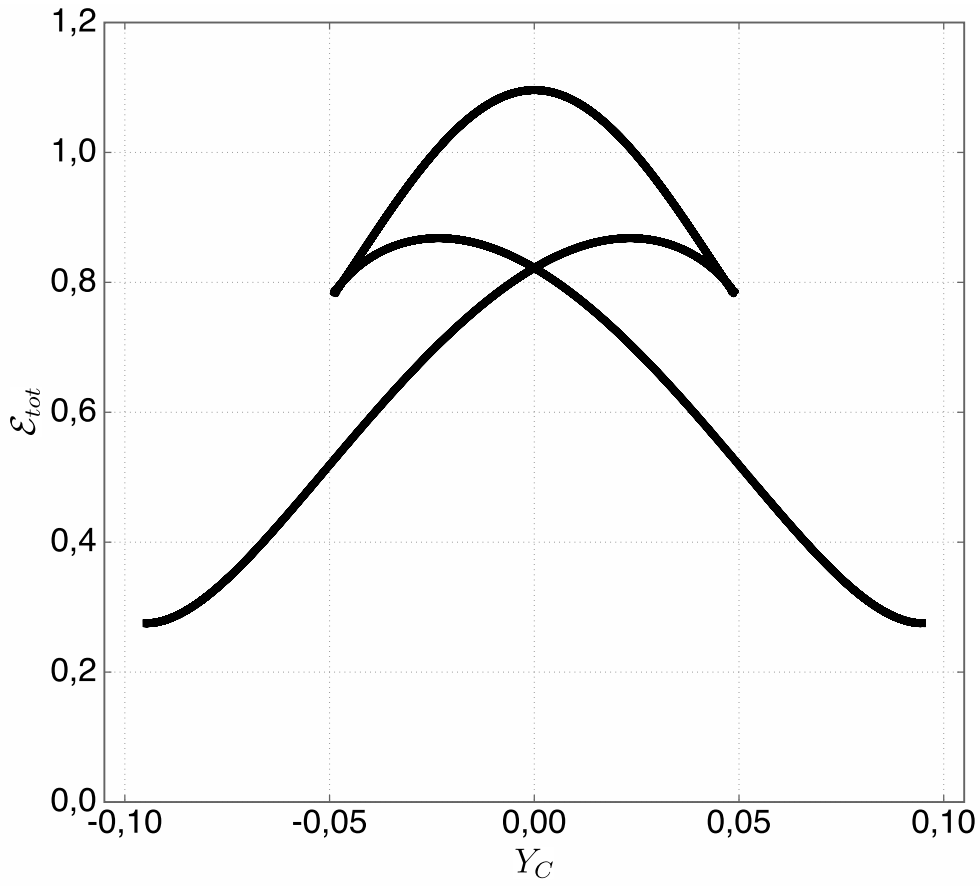

Figure 11: The total energy as function of the position Y_C (non-central actuation at 39 %) (for $k = 1/2500$ and $\Delta\mathsf{L} = 0.03$).

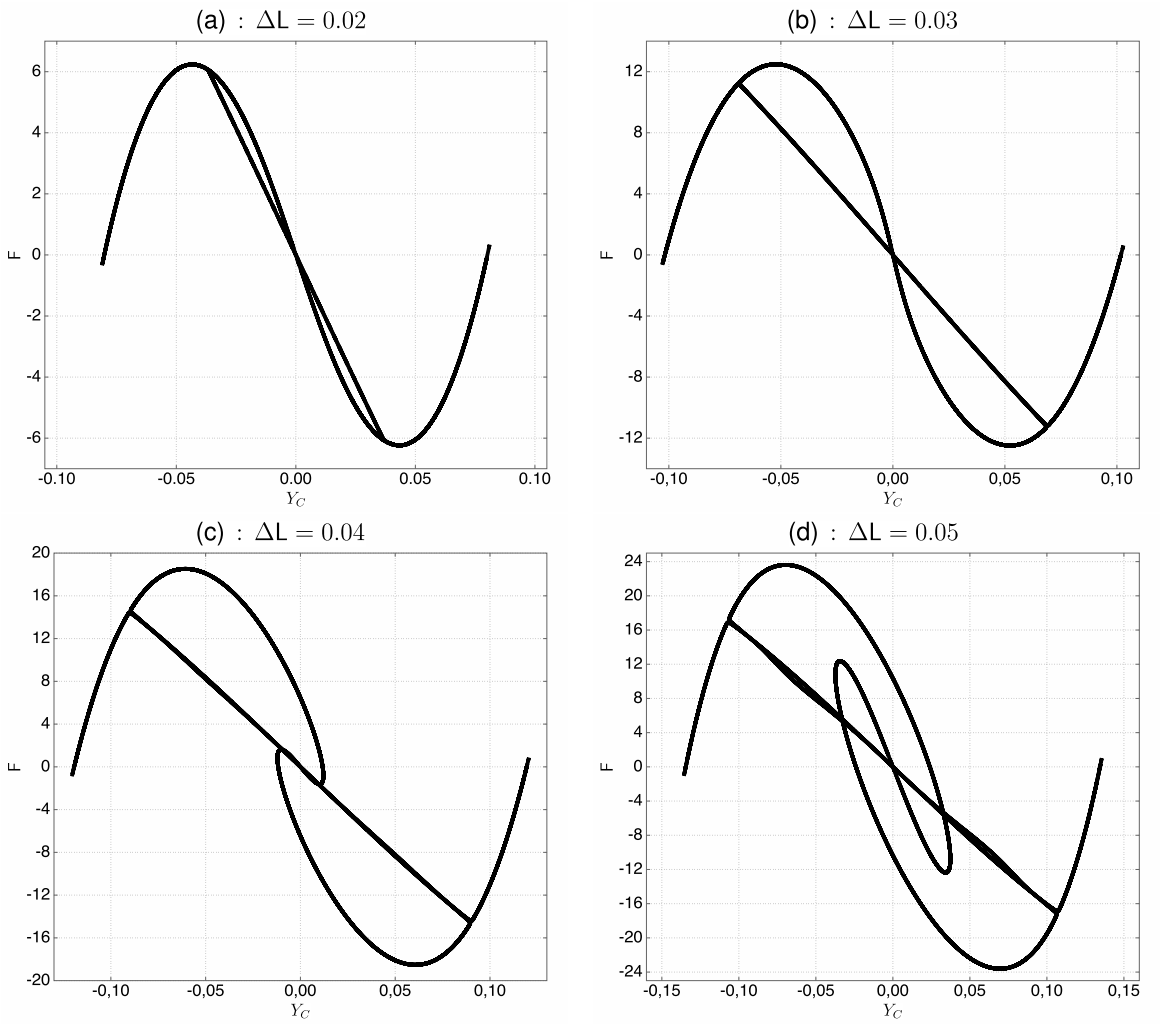

Figure 12: Influence of the end-shortening of right end of the beam on the bistable buckled beam response, actuating force v.s. the position Y_C (for central actuation $\hat{\delta} = 0.5$, $k = 1/2500$) : (a) $\Delta L = 0.02$, (b) $\Delta L = 0.03$, (c) $\Delta L = 0.04$ and (d) $\Delta L = 0.05$.

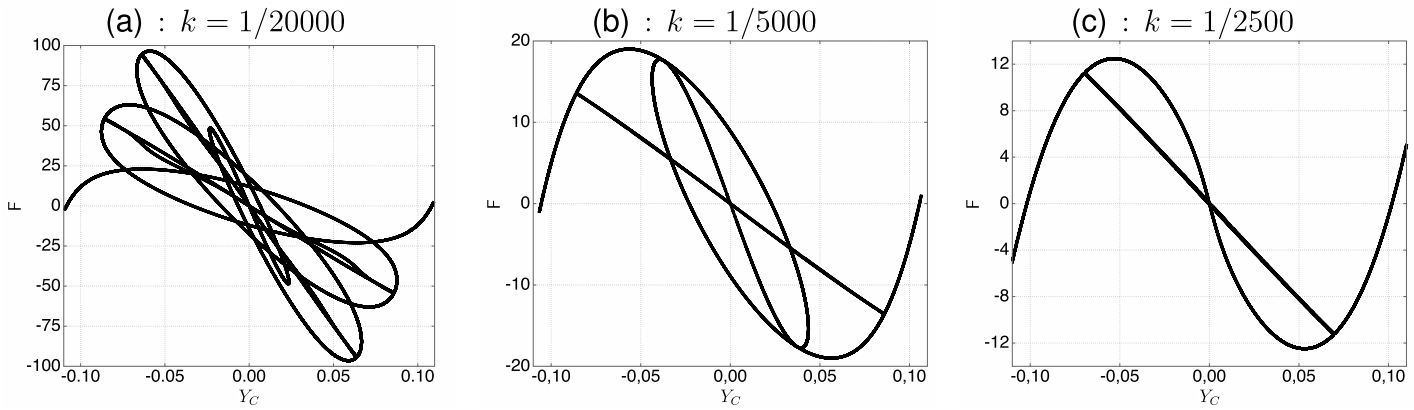

Figure 13: Influence of the extensibility parameter k on the bistable buckled beam response, actuating force (in Newton) v.s. the position Y_C (for central actuation and $\Delta \mathsf{L} = 0.03$) : (a) $k = \frac{1}{20000}$, (b) $k = \frac{1}{5000}$ and (c) $k = \frac{1}{2500}$.

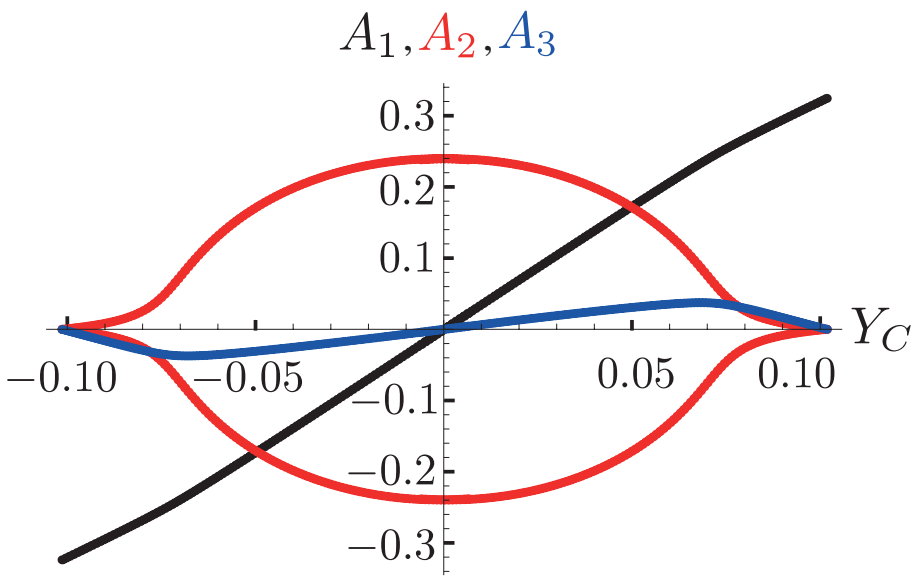

Figure 14: The amplitudes of the first three buckling modes as function of the actuating force vertical displacement (black : A_1, red : A_2, blue : A_3) for $k = \frac{1}{2500}$, $\Delta \mathsf{L} = 0.03$ and central actuation.

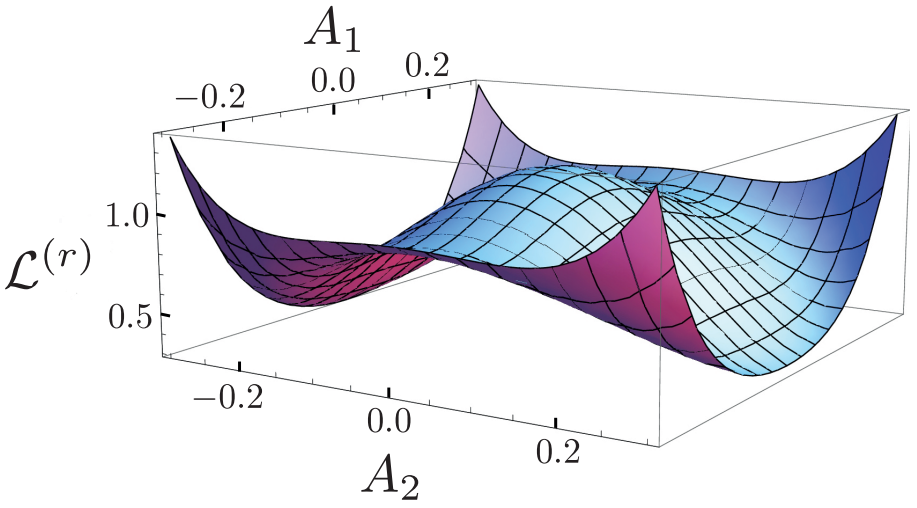

Figure 15: The 3D plot of the beam Lagrangian functional in the $(A_1 - A_2)$-plane. The graph displays (i) two stable equilibrium positions, (ii) one unstable equilibrium position at $(0, 0)$ and (iii) two saddle points.

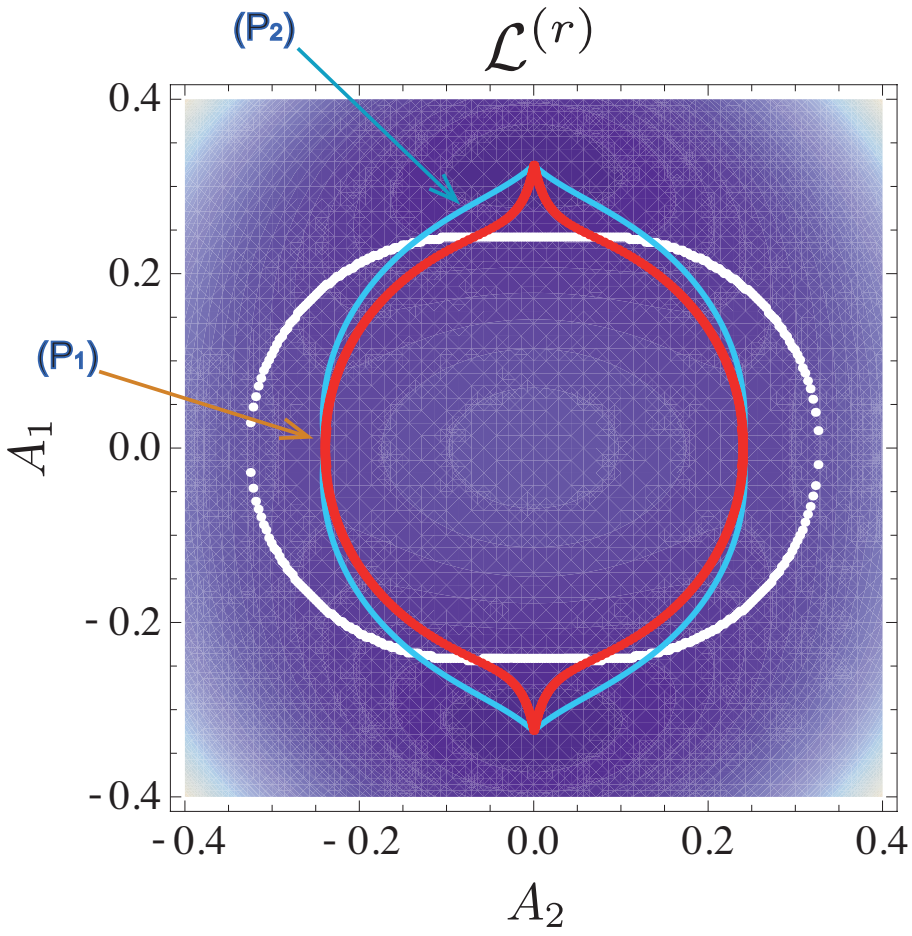

Figure 16: The contourplot of the bistable Lagrangian functional. The white closed curve is the limit of the instability region. The red curve corresponds to the central actuation and the blue curve is for shifted actuation at 39 %.